University of Texas Rio Grande Valley
ScholarWorks @ UTRGV

Theses and Dissertations - UTRGV

8-2023

Simple Mechanically Reconfigurable Patch Antennas

Luis Alonso Hernandez Galvan
The University of Texas Rio Grande Valley

Follow this and additional works at: https://scholarworks.utrgv.edu/etd

Part of the Electrical and Computer Engineering Commons

Recommended Citation

Hernandez Galvan, Luis Alonso, "Simple Mechanically Reconfigurable Patch Antennas" (2023). *Theses and Dissertations - UTRGV*. 1353.
https://scholarworks.utrgv.edu/etd/1353

This Thesis is brought to you for free and open access by ScholarWorks @ UTRGV. It has been accepted for inclusion in Theses and Dissertations - UTRGV by an authorized administrator of ScholarWorks @ UTRGV. For more information, please contact justin.white@utrgv.edu, william.flores01@utrgv.edu.

SIMPLE MECHANICALLY RECONFIGURABLE PATCH ANTENNAS

A Thesis

by

LUIS ALONSO HERNANDEZ GALVAN

Submitted In Partial Fulfillment of the

Requirements for the Degree of

MASTER OF SCIENCE IN ENGINEERING

Major Subject: Electrical Engineering

The University of Texas Rio Grande Valley

August 2023

SIMPLE MECHANICALLY RECONFIGURABLE PATCH ANTENNAS

A Thesis
by
LUIS ALONSO HERNANDEZ GALVAN

COMMITTEE MEMBERS

Dr. Nantakan Wongkasem

Chair of Committee

Dr. Teviet Creighton

Committee Member

Dr. Heinrich Foltz

Committee Member

Dr. Yong Zhou

Committee Member

August 2023

Copyright 2023 Luis Alonso Hernandez Galvan

All Rights Reserved

ABSTRACT

Hernandez Galvan, Luis A., Simple Mechanically Reconfigurable Patch Antennas. Master of Science (MS), August, 2023, 76 pp., 14 tables, 44 figures, 37 references, 34 titles.

Reconfigurable antennas form an active subdivision of antenna and communications research primarily targeted at achieving reconfigurability in the RF, microwave, and millimeter-wave frequency regimes. Mechanical, all-electronic, material based, and optical methods are the most common approaches to achieve reconfigurability. Each method can overlap to create new and innovative approaches to enable device tunability. The sub-class of reconfigurable antennas are antennas that dynamically achieve an adaptable transformation of their frequency, radiation-pattern, polarization, and/or bandwidth characteristics to enable multiple dynamic functionalities.

In this thesis, we designed new rectangular and triangular microstrip patch array antennas operating in the 5G midband at 5GHz. These patch antennas were designed and inspired by the Yagi-Uda antenna, where the driven and passive director or parasitic patches are the main elements. It was found that by increasing the number of parasitic elements, the antenna's gain can be improved, despite some impedance mismatch. The triangular patch array with the best result was then selected to further investigate its reconfigurability capability using two simple mechanically reconfigurable approaches, i.e., 1) single-plane and 2) double-plane patch arrays, focusing on the radiation pattern, gain, and operating frequency, and other antenna performances. The single-side and double-side folded structures were examined in both approaches, while the

folded feeding line and curvature folded substrate were also studied in the single-plane patch array. The results provided clear evidence that by folding the substrate at varying angles one can effectively manipulate the antenna's radiation pattern, gain, and center operating frequency location. The impact varies with the degree of folding, signifying a direct relationship between the folding angle and the returning loss or S_{11} value. Three proposed microstrip array antennas, i.e., the single-plane patch antenna array, the triangle microstrip array, and the microstrip Yagi-Uda antenna array, were fabricated and tested. The simulation and measurement results are in good agreement.

DEDICATION

To My Family:

My dad who supports me every step along the way, my mom who always believes in me, my brother and his wife who encourage me to improve my knowledge, and last, but not least, to my beautiful fiancée who brings me the motivation and shows me the meaning of life in hard times.

ACKNOWLEDGMENTS

I'm thankful with the members of the CARA Executive Committee, Dr. Creighton, and Dr. Quetschke for the support in the projects related in the center and the funding provided for my research assistantship through my master's. Also, I am grateful for the guidance provided by my advisor from the Department of Electrical and Computer Engineering, Dr. Nantakan Wongkasem for her advising, knowledge, and patience given to me during my project.

Thanks to all my research mates, Luis Bres, Francisco Llamas, Aram Flores, Yhamil Garcia, Alex Corona, Rhobenn Jericho for being in my journey and helping me around the way.

I thank the Department of Electrical and Computer Engineering at the University of Texas Rio Grande Valley for providing the setting and support that allowed this work to be done and for providing preparation for this thesis and my degree. Thanks to CARA and the Physics Department for the research positions provided so that I could continue pursuing my career.

TABLE OF CONTENTS

Page

ABSTRACT…… iii

DEDICATION…… v

ACKNOWLEDGMENTS…….. vi

TABLE OF CONTENTS…… vii

LIST OF TABLES……..…. x

LIST OF FIGURES…… xi

CHAPTER I. INTRODUCTION……..... 1

1.1 Reconfigurable Antennas…….…… 1

1.2 Proposed Reconfigurable Antennas.…….…….……..... 8

CHAPTER II. MICROSTRIP ANTENNA DESIGN AND ANALYSIS ……..…..… 10

2.1 Rectangle Microstrip Calculation.……....… 11

2.2 Triangle Microstrip Analysis.…..……..…… 14

2.3 Microstrip Yagi Array Design.…..…….……..... 15

2.4 Triangle Microstrip Design.…..…….……..... 17

CHAPTER III. SIMULATION AND COMPARISON OF ANTENNA RESPONSE…….. 19

3.1 Rectangular and Triangular Array Response Comparison…..……. 20

3.2 1st Approach: Single Plane Folded Patch…… 21

3.3 1st Approach: Single-Plane Folded Patch Antenna Study.……....……. 23

3.3.1 One-Side Unfolded Microstrip Line Simulation

Response…….……...……..... 24

3.3.2 Two-Sides Unfolded Microstrip Line Simulation

Response.…….……...……. 27

3.3.3 One-Side Folded Microstrip Line Simulation

Response……..……..…….……...……. 29

3.3.4 Two-Side Folded Microstrip Line Simulation

Response ...…….……...……. 32

3.3.5 Curvature Folded Substrate. …..…….…….....……. 36

3.4. 2nd Approach: Double-Plane Patch..……..…….…….....……. 37

3.4.1 Single-folded Director Study Response……..……. 37

3.4.2 Double-folded Director Study Response…….……..... 44

CHAPTER IV. FABRICATION AND MEASUREMENTS……..……..... 47

4.1 Fabrication Process with LPKF ProtoLaser Machine…..…….....……. 37

4.2 Measurements…….…….....……..... 52

CHAPTER V. FINDINGS AND COMMENTS ……..…….…… 59

5.1 Rectangular and Triangular Array Response Comparison…… 59

5.2 1st Approach: Single Folded Patch Antenna Study…… 60

5.2.1 One-Side Unfolded Microstrip Line

Findings and Comments…….. 61

5.2.2 Two-Sides Unfolded Microstrip Line

Simulation Response……..…….…… 62

5.2.3 One-Side Folded Microstrip Line

Simulation Response…….…….. 62

5.2.4 Two-Side Folded Microstrip Line

Simulation Response…….. 63

5.2.5 Simulation of Curvature Folding Substrate……..... 64

5.3. 2nd Approach: Double-Plane Patch……. 65

5.3.1 Single-Folded Director Study Response……..……. 65

5.3.2 Double-Folded Directors Study Response……..…….. 66

REFERENCES…….. 72

BIOGRAPHICAL SKETCH……. 76

LIST OF TABLES

Page

Table 1.1 Reconfigurable antennas and our proposed Yagi-inspired patch before folding (Q and R.)…….…….. 4

Table 2.1 Rectangular microstrip array parameters ……..…… 16

Table 2.2 Triangle microstrip array dimensions ..……. 18

Table 3.1 Rectangular and triangle array response...……...…….. 21

Table 3.2 1st Approach: single-plane, single-folded patch study……..... 25

Table 3.3 1st Approach: single-plane, double-side folded patch response……..... 28

Table 3.4 Single-side folded microstrip line simulation response……...…..……..…..... 30

Table 3.5 Double-side folded microstrip line simulation response.……..……..…..... 33

Table 3.6 2nd Approach: Double-plane patch, design dimensions…...…..……..…..... 39

Table 3.7 2nd Approach: Double-plane single director folded patch simulation response……..…...……..…..... 41

Table 3.8 2nd Approach: Double-plane, double-folded director simulation response...…..…..... 44

Table 4.1 Software procedures for LPKF laser U4…….……..... 49

Table 4.2 Calibration process of vector network analyzer ….…….……..... 55

Table 4.3 S_{11} parameters: comparison between simulation vs measured results…….…..... 56

LIST OF FIGURES

Page

Figure 1.1 Folded substrate configurations of proposed antenna first design.……8

Figure 1.2 Design of parasite elements in driven elements parallel plane……..……9

Figure 2.1 Rectangular and triangular microstrip ….……..……..10

Figure 2.2 Triangular Patch ……..14

Figure 2.3 Rectangular Microstrip Array ……..15

Figure 2.4 Triangular Microstrip Array ..……..17

Figure 3.1 1st Approach: Single-plane folded patch CST design...…….…..22

Figure 3.2 1st Approach: Single plane folded patch far-field response..……...23

Figure 3.3 1st Approach: Single-plane folded patch S11 response…...……...23

Figure 3.4 1st Approach: Single-plane folded patch one side at 15°.....……..25

Figure 3.5 S_{11} parameters of one side folded without folding microstrip line……..27

Figure 3.6 1st Approach: Single-plane folded patch, two side folded at 15°…….…...27

Figure 3.7 S_{11} parameters of two side folded with folding microstrip line…….…..30

Figure 3.8 1st Approach: Single-plane folded patch, one side folding with microstrip line at 15°……..……...…….30

Figure 3.9 S_{11} parameters of one side with folding microstrip line.……..…….…...32

Figure 3.10 1st Approach: Single-plane, two side folding with microstrip line at 15°……...…..33

Figure 3.11 S_{11} response of double-side folded microstrip line ……..…...…..35

Figure 3.12 Semicircular folding 1st Approach: Single-plane folded patch ……..…...…..36

Figure 3.13 1st Approach: Single-plane semicircular folding far-field and polar response……..37

Figure 3.14 2nd Approach: Double-plane patch, directors parallel to the plane of driven elements……..38

Figure 3.15 2nd Approach: Double-plane patch, design dimensions.……...…...…..39

Figure 3.16 S11 2nd Approach: Double-plane patch response…….……...…...…..39

Figure 3.17 Far-field of 2nd Approach: Double-plane patch response……..…...…..40

Figure 3.18 Polar chart of 2nd Approach: Double-plane patch response …….……..…...…..40

Figure 3.19 S_{11} of 2nd Approach: Double-plane patch with one director folding response.…..……..……..…..43

Figure 3.20 Gain vs theta 2nd Approach: Double-plane patch response.…….....…..43

Figure 3.21 S_{11} of 2nd Approach: Double-plane patch, both folded directors response……...…….……...…..46

Figure 3.22 Gain vs theta, 2nd Approach both folded directors response.……...…….46

Figure 4.1 LPKF ProtoLaser U4…….……...…....48

Figure 4.2 Fabricated 1st Approach: Single-plane folded patch..……...……..48

Figure 4.3 Antennas array fabricated with LPKF U4……..…….……...…..…..51

Figure 4.4 Fabricated 1st Approach: Single-plane folded patch when folds.……...…..…..52

Figure 4.5 Calibration kit HP 85052B ……..…….……...…..……....54

Figure 4.6 Calibration kit components ……..…….……...…..……54

Figure 4.7 Testing setup.……..…….……...…..……...…...54

Figure 5.1 1st Approach: Single-plane folded patch……..61

Figure 5.2 1st Approach: Single-plane folded patch one side……62

Figure 5.3 1st Approach: Single-plane folded patch, two side folded……63

Figure 5.4 1st Approach: Single-plane folded patch, one side folding with microstrip line……...64

Figure 5.5 1st Approach: Single-plane, two side folding with microstrip line……..65

Figure 5.6 Semicircular folding 1st Approach: Single-plane folded patch……66

Figure 5.7 2nd Approach: Double-plane patch, directors parallel to the plane of driven elements……..68

Figure 5.8 2nd Approach: Double-plane patch, single side folding……69

Figure 5.9 2nd Approach: Double-plane patch, double side folding……...70

CHAPTER I

INTRODUCTION

1.1 Reconfigurable Antennas

The first antennas were built in 1888 by German physicist Heinrich Hertz in his experiments to prove the existence of waves predicted by the electromagnetic theory of James Clerk Maxwell. Since then, antennas have been a widely discussed field and played a significant role in wireless communications. Antenna reconfiguration of different parameters is the main objectives and study goal for several applications, e.g., space, communication technologies, etc. Antenna design depends on the purpose for which the antenna will be used. Different antenna configurations are manipulated to fit in based on the usage [1, 3, 14].

Reconfigurable electromagnetic devices, specifically reconfigurable antennas, have shown to be integral to the future of communication systems. The comprehensive subject of reconfigurable electromagnetic devices has become the recent focus of active research [2, 4, 10, 15, 20,]. Reconfigurable antennas form an active subdivision of antenna and communications research primarily targeted at achieving reconfigurability in the RF, microwave, and millimeter-wave frequency regimes. Current reconfigurable antenna solutions can be classified according to their method of achieving actuation. While [2] mechanical, [20] all-electronic, [4] material based, and [15] optical methods represent the most common approaches to achieve reconfigurability, each

can overlap to create new and innovative methods to enable device tunability. The sub-class of reconfigurable antennas are antennas that dynamically achieve an adaptable transformation of their frequency, radiation-pattern, polarization, and/or bandwidth characteristics to enable multiple dynamic functionalities. One of the first reconfigurable antenna systems was published in 1935 [8]. It was shown that the radiation pattern of a rhombic antenna can be modified by adjusting counterweights which vary the wire element angles, therefore changing the resultant radiation pattern. Cognitive radio applications antennas are commonly designed to have a reconfigurable frequency to enable dynamic spectrum access and adapt to changing environmental conditions [9, 30]. Meanwhile reconfiguration of radiation pattern is used for mobile antennas to optimize the signal strength and directionality based on the changing orientation and location of the antenna [34, 36]. Portable devices use reconfiguration of their polarization to reduce the impact of signal attenuation caused by the polarization mismatch with surrounding objects and improve the signal quality [19, 32]. An antenna can have a hybrid reconfiguration when spectral efficiency needs to be improved, by combining frequency and radiation pattern reconfigurations to optimize the use of available spectrum and enhance the signal quality [21].

The field of reconfigurable antennas can facilitate the reduction of the hardware bottleneck by allowing multi-functions to co-exist within a single antenna. Further advancements, such as, lessened hysteresis between configuration states, long mean time between failures and high-power handling can help maximize performance of reconfigurable antennas. Moreover, it is desired to extend the operational capabilities as these improvements can lead to a lowering of system costs by reducing the number of required onboard components and devices [6, 13, 22, 37].

One of the most popular types of mechanically reconfigurable antennas are those referred to as Origami Antennas (OA) as they take their inspiration from the Japanese art of paper folding.

Origami antennas have been implemented in extensive ways, ranging from helical antennas capable of switching their radiating pattern polarization [33], reducing system costs by utilizing paper as a substrate structure [28], and frequency selective surfaces and deployable reflecting surfaces [5-26]. The main drawback of OAs is that specific behaviors and material performance assumptions need to be made to realize targeted functionality. Some of these limitations include requiring a sufficiently thin target substrate with negligible elasticity and that the folding section includes motion not along substrate folds. Moreover, if the substrate thickness is increased to improve mechanical rigidity, then the problem of self-avoidance or non-self-intersection starts to play an ever-increasing role [18]. Other limitations of OAs include structures and patterns that are not typically rigid/robust for field deploy ability and are limited in their stacking and implementation into three dimensional structures. Also, due to the propensity to use thin, flexible substrates there is minimal force amplification available to create actuation devices [24-35].

Based on current reconfigurable antenna solutions, antenna structure, parameters and geometries can change, and can provide tunability, reconfigurability, and multi-band operation. This allows for compact and lightweight designs and enables the creation of complex radiation patterns that are difficult to achieve with traditional antenna designs [12], with the constraint that depending on the origami design external actuators can be needed. Thus, folded antenna design has become a trend in different applications like microstrip patch antennas (MPA) where origami-folded concept can be easily adapted with the use of thin substrates and meta-materials [14,29]. Conformal MPA, a type of antenna that is designed to conform to the shape of the surface on which it is mounted, [7, 23, 31], uses not origami but folded structures for aeronautical and mobile applications. MPA arrays that can fold into origami structures, can change different parameters depending on design, it can benefit with high gain, directional radiation pattern, low profile, and

ease of integration with other electronic components [27], this can be implemented in space communications for CubeSats and satellites due to their ability to be compactly stowed for launch and then deployed into large structures, providing greater aperture and thus better performance for communication systems [16-25]. It was proved that as the folded angle increases, the array beamwidth increases and the gain decreases. Also, the matching impedance of the array degrades with increased fold angle [11]. It has been shown that MPA can have an easily adaptability to all these configurations and designs, but also, can be adapted to control the beam pattern as a Yagi-Uda form [17]. in this configuration the radiation it is controlled by a driven cooper printed element and both reflector and director parasite elements. With this model, gain and directivity are improved but the radiation of this design is fixed, once designed cannot change their configuration.

Table 1.1 shows the most recent reconfigurable antennas published by different research groups. Antenna images, dimensions, reconfiguration type, design, and operating frequency range are also listed. The last two antennas (Q. and R.) are our proposed Yagi inspired patch antenna before folding to create the mechanic reconfiguration.

Table 1.1 Reconfigurable antennas and our proposed Yagi-inspired patch before folding (Q and R.)

Antenna	Reconfiguration Type	Design	Freq.	Refs
A. 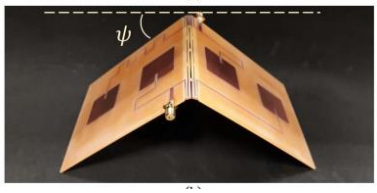 Dimensions: 250 x 102 x 1.5mm.	Beam steering. Scan angles greater than 35◦ when folded.	MPA, FR4 substrate folded.	2.4 GHz	[14]
B. Dimensions: 552 x 35.3 x 4.5 mm.	Multi-band. Operation band is adjusted by changing its height.	Origami multi-radii monofilar helical antenna.	1.2-1.5 GHz 2.3-3.5 GHZ	[30]

Table 1.1., Cont.

C. 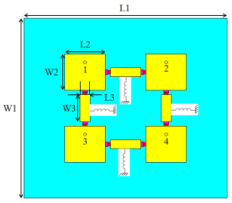 Dimensions: 31 x 35 x 1.6 mm.	Reconfigurable frequency.	MPA array 2x2, PIN diode.	3.4 GHz to 12.1 GHz.	[9]
D. Dimensions: 148 x 32 mm.	Change from omni-directional to directional. radiation pattern.	Two-arm Nojima origami conical spiral antenna (CSA).	UHF and 1.5 GHz.	[34]
E. 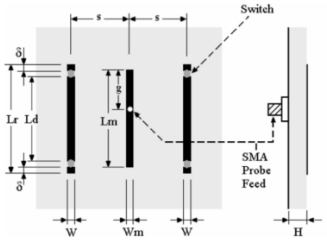 Dimensions: 50 x 50 x 6.35 mm.	Radiation pattern. From 25◦ to 45◦.	4 cooper strip switches.	3.6 GHz	[36]
F. 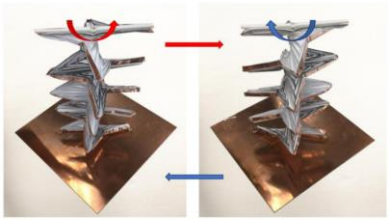 Dimensions: 672 x 160 x 5 mm.	Polarization switch.	Origami Segmented Helical Antenna.	UHF	[32]
G. 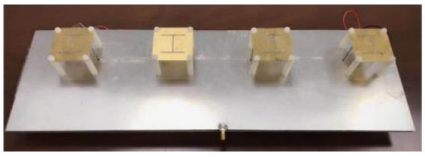 Dimensions: 400 x 120 x 0.8 mm.	Polarization switch.	1x4 antenna array.	2.4 GHz	[19]
H. 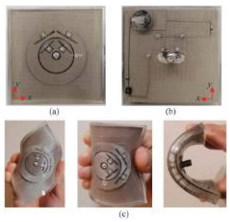 Dimensions: 70 x 70 x 6.6 mm.	Physical.	Conductive Textile-Polymer Composite.	5.2 GHz	[23]

Table 1.1., Cont.

I. Dimensions: 36.5 x 43.6 x 1.3 mm.	Physical.	MPA array.	2.45 GHz	[7]
J. 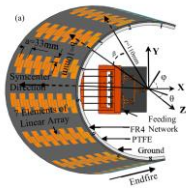 Dimensions: 109 x 229 x 0.254 mm.	Angle Beam Switching.	Conical Conformal Array.	4.8 GHz	[31]
K. 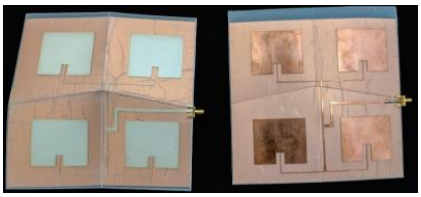 Dimensions: 160 x 160 x 0.75 mm.	Physical.	Origami MPA array.	2.4 GHz	[27]
M. 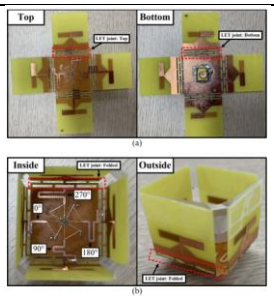 Dimensions:100 x 100 x 0.5 mm.	Radiation pattern and physical.	Origami dipole array antenna.	5.8 GHz	[16]
N. 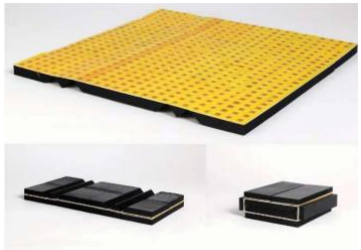 Dimensions: 230 x 230 x 0.812 mm.	Physical.	Foldable reflect array antenna.	16 GHz	[25]
O. 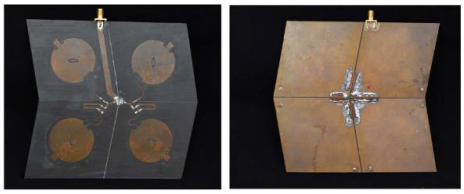 Dimensions: 130 x 130 x 1.5748 mm.	Radiation pattern and physical.	Circular patch array, switch ON/OFF.	3 GHz	[11]

Table 1.1., Cont.

P. 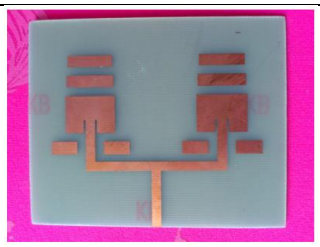 Dimensions: 65 x 80 x 1.6 mm.	Radiation pattern.	MPA array and passive elements.	5.5 GHz	[17]
Q. 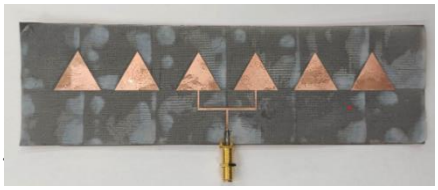 Dimensions: 200 x 60 x 0.254 mm.	**Proposed Antenna 1** **Radiation pattern/Mechanic**	MPA array, passive in the same plane as driven elements, and folding structure.	5.8 GHz	
R. 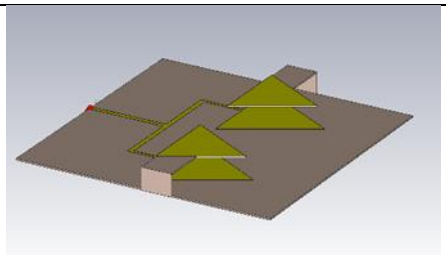 Dimensions: 60 x 60 x 0.254 mm.	**Proposed Antenna 2** **Radiation pattern/Mechanic**	MPA array, passive parallel to the driven elements plane, and folding structure	5.8 GHz	

To design a physical origami-inspired/folded reconfigurable antenna, the most common approach is with the use of MPA arrays and thin substrates that can fold. To achieve that, it must be considered concepts, for example, matching impedance, when antenna arrays are designed given that each microstrip irradiates an impedance that must match with the others when connected via microstrip copper lines. Also, it is essential to understand that contrary to regular antennas that use air to receive electromagnetic waves (EM), EM waves travel through the substrate in MPA.

This produces a mismatch impedance in the design when folding microstrip connection lines are folded in origami structures, causing a little offset in the original frequency, or reducing efficiency. Also, in case of the origami/folding design, it is important to decide the form and patrons of the structure to achieve whichever reconfiguration. In this matter, it is important to calculate and decide MPA array positions, microstrip connections, type on antennas, substrate, and folding arrangements to accomplish the design goals.

1.2 Proposed Reconfigurable Antennas

In this research, a simple mechanically reconfigurable antennas are designed, fabricated, and tested. Reconfigurable microstrip antenna design and analysis is discussed in Chapter 2. Simulation and comparison of antenna response are described in Chapter 3, fabrication, and testing results are presented in Chapter 4. Research discussion and future work are in Chapter 5. Figure 1.1 shows the examples of folded substrate configuration of proposed patch antennas.

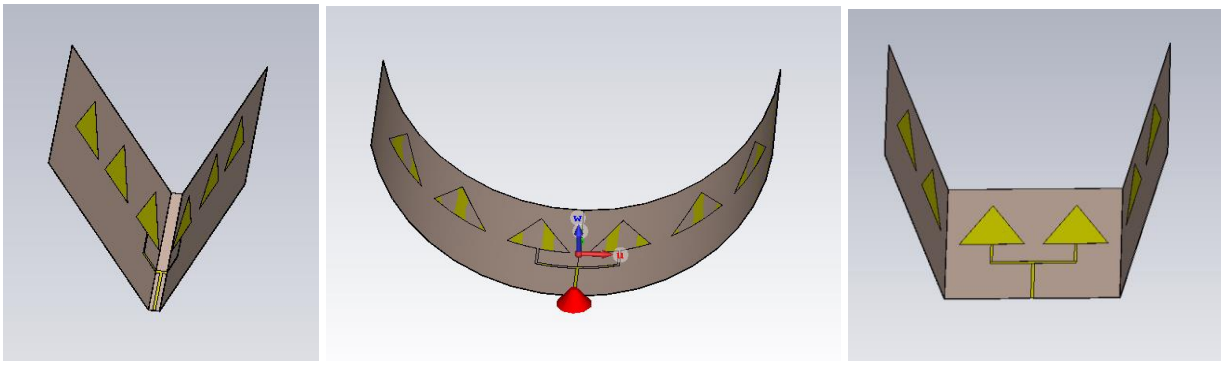

Figure 1.1 Folded substrate configurations of proposed antenna first design

The antenna array consisting of six elements, with two elements in the middle acting as driven elements and two on each side serving as parasitic elements. The main objective of this thesis is to study the effects of parasitic elements on the radiation pattern when the substrate is folded. Special attention is given to the impact on S_{11} parameter responses when a microstrip line connecting the driven elements is folded. The fabrication, testing, and measurement of this design are presented in later chapters.

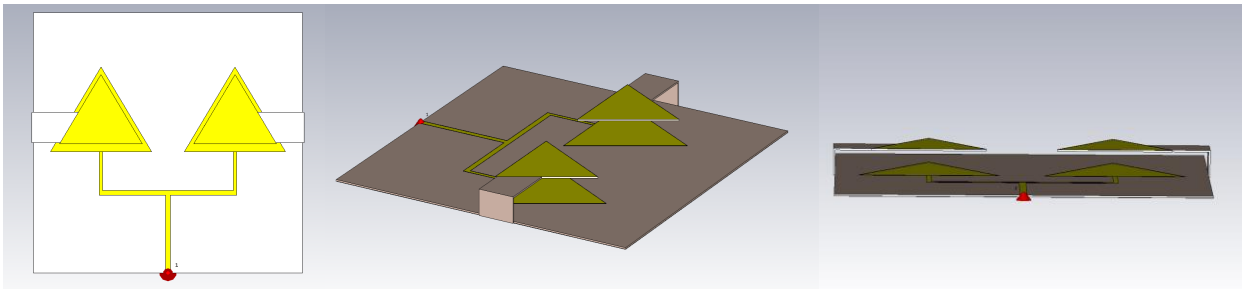

Figure 1.2 Design of parasite elements in driven elements parallel plane

Figure 1.2 presents double-plane Yagi inspired patch before folding. Unlike the design in Figure 1.1, the directors are placed on top of the driven element plane, mimicking a Yagi-Uda antenna. In this configuration, the ground plane acts as a reflector, the driven elements are at a separation distance, and the directors face the driven elements, resulting in a reduction of 15% in size. This size reduction produces a lens reflection effect that focuses the beam. The response of this design is simulated and compared with the response of the previous design. Additionally, a study of the beam pattern control is conducted by folding the directors at different angles.

CHAPTER II

MICROSTRIP ANTENNA DESIGN AND ANALYSIS

A microstrip patch antenna is a type of antenna that has gained significant popularity in recent years due to its low profile, ease of fabrication, and versatility. It is widely used in various applications such as wireless and satellite communications, and radar systems, to name a few. The performance of a microstrip patch antenna is highly dependent on its geometrical parameters and the dielectric properties of the substrate material used. Therefore, a thorough analysis of the antenna's design is crucial to ensure its optimum performance. In this research, we present a detailed analysis of a microstrip patch antenna, including its design, simulation, and experimental results. The aim of this study is to evaluate the performance of the antenna and optimize its design parameters to achieve a desired level of performance. Figure 2.1 presents two simple patches: rectangular and triangular shapes.

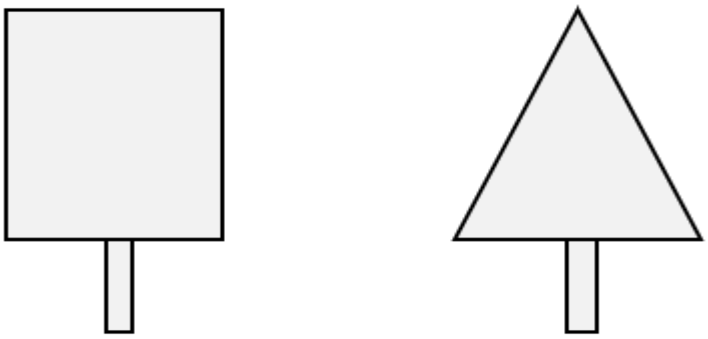

Figure 2.1 Rectangular and triangular microstrip.

The report begins with an introduction to the basic concepts of microstrip patch antennas, followed by a detailed description of the antenna design and simulation methodology. Finally, the experimental results are presented and analyzed to validate the simulation results and evaluate the performance of the antenna.

2.1 Rectangle Microstrip Calculation

The first step of the design procedure is started by designing a single element. This element is a rectangular microstrip patch of one branch which is called a driven element. It is designed to operate at a resonant frequency, f_r= 5.8 GHz using HR700 substrate material. The dielectric constant of the substrate is ε_r= 3.92, thickness of the substrate h = 0.9906 mm. The physical width and length dimensions of the driven patch element are calculated using the following equations [1-].

$$W = \frac{C}{2f\sqrt{\varepsilon_r}}\left(\sqrt{1-\left(\frac{h-t}{h+t}\right)^2}+1\right) \tag{2.1}$$

where,

C is the speed of light in vacuum or free space = $\frac{1}{\sqrt{\varepsilon\mu}}$;

f is the operating frequency of the antenna;

ε_r is the effective dielectric constant of the substrate material;

H is the substrate height; and

T is the conductor thickness.

Note that this formula assumes a rectangular microstrip patch element with an infinite ground plane, and it is commonly used to calculate the optimal width of the patch for a given set of design parameters.

$$\varepsilon_{reff} := \frac{\varepsilon_r+1}{2} + \frac{(\varepsilon_r-1)}{2}\left(1 + 12\left(\frac{h}{w}\right)^{\frac{1}{2}}\right)^{-\frac{1}{2}} \tag{2.2}$$

where,

ε_r is the relative permittivity (dielectric constant) of the substrate material.

h is the substrate height.

w is patch width.

ε_{reff} is the effective dielectric constant of the microstrip patch antenna.

The formula is used to calculate the effective dielectric constant for a rectangular microstrip patch antenna. By varying the values of ε_r, h, and w, antenna engineers can optimize the antenna's resonant frequency, bandwidth, and impedance characteristics to suit their application. The relative permittivity of the substrate material on which the microstrip patch antenna is mounted. Relative permittivity is a measure of the ability of the material to store electric charge in an electric field, and it affects the speed of electromagnetic wave propagation through the material. The height of the substrate, which is the thickness of the patch in the direction perpendicular to the ground plane.

The width of the patch, which is the dimension of the patch in the direction parallel to the ground plane. The effective dielectric constant of the microstrip patch antenna. This is the value that considers the effect of the substrate material on the electromagnetic field distribution and the effective dimensions of the patch and is used to determine the resonant frequency and impedance characteristics of the antenna.

The actual length, L of the patch can be determined as follows:

$$L = \frac{c}{2f\sqrt{\varepsilon_r}}\left(1 - \frac{1}{2(\varepsilon_r+1)}\right) - \frac{0.064}{f\sqrt{\varepsilon_r}}\left(\frac{h}{W} + 1.25\right) \tag{2.3}$$

where,

C is the speed of light in vacuum;

f is the operating frequency of the antenna;

ε_r is the effective dielectric constant of the substrate material;

h is the substrate height;

W is the patch width.

$$\lambda_g = \frac{\lambda_a}{\sqrt{\varepsilon_{reff}}} \tag{2.4}$$

λg is the guide wavelength of an electromagnetic wave propagating through a microstrip transmission line. This wavelength is determined by the physical dimensions of the transmission line and the properties of the material it is made of.

λa is the free-space wavelength of the electromagnetic wave, which is the wavelength of the wave if it were propagating through free space with no medium present.

ε_{reff} is the effective dielectric constant of the microstrip transmission line. This is a value that considers the effect of the substrate material and the physical dimensions of the transmission line on the electromagnetic wave propagation. It is used to determine the characteristic impedance, propagation constant, and other properties of the transmission line.

2.2 Triangle Microstrip Analysis

The initial stage of the design process involves creating a single element using a triangular microstrip patch instead of a rectangular one. This triangular microstrip patch serves as a driven element and is designed to operate at a resonant frequency of f_r = 5.8 GHz. The HR700 substrate material with a dielectric constant of ε_r= 3.92 and a thickness of h = 0.9906 mm is utilized for this design. The physical width and length dimensions of the driven patch element are calculated using the equations provided in references [1-3].

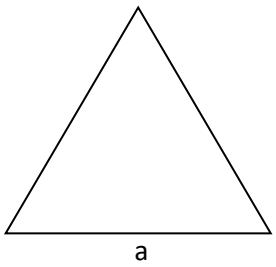

Figure 2.2 Triangular Patch.

$$\mathrm{a} = \frac{2\mathrm{c}}{3f_r\sqrt{\varepsilon_r}} \tag{2.5}$$

$$f_r = \frac{2c}{3a\sqrt{\varepsilon_r}} \tag{2.6}$$

where:

f_r is the resonant frequency of the triangular microstrip antenna.

c is the speed of light in free space.

a is the length of one side of the triangular patch.

$\varepsilon_r$is the dielectric constant of the substrate.

2.3 Microstrip Yagi Array Design

The above diagram illustrates a microstrip Yagi antenna with two branches, which includes two driven patch elements and several director and reflector patch elements coupled parasitically. The driven element, denoted as *D*, is excited through a small gap of the reflector elements by a

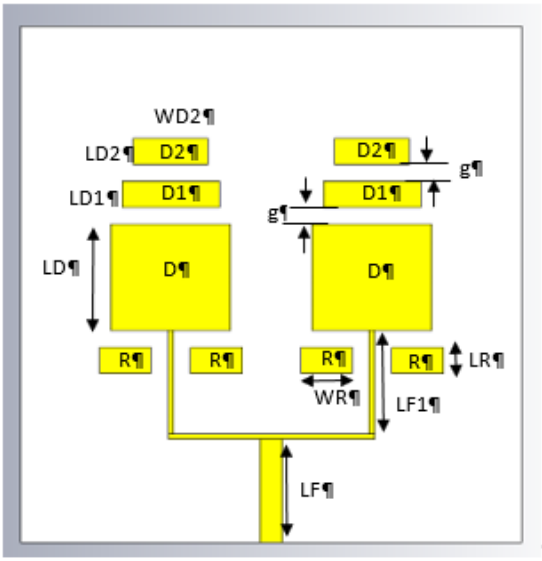

Figure 2.3 Rectangular Microstrip Array.

simple feeding structure. The reflector elements, R, are treated as a single element with a gap in the middle of the feeding element. A 50 Ω microstrip feedline is utilized as the feeding structure, which is connected to the center of the driven element through a quarter-wave transformer. In addition to establishing the directionality of the beam, two directors, D1 and D2, are employed to increase the antenna gain.

Table 2.1 Rectangular microstrip array parameters.

Parameter	Value	Description
LR	RW/2	Reflector length
LF = LF1	lambda/4	Patch link length
TL = TW	60	Total length and width
lambda	47.91	lambda/2
D	14	Patch width
LD	12.3	Patch length
InW	2.63	Input link width
PinW	0.64	Patch link width
D1	9.44	Director length
LD1	3.64	Director' width
g	1.98	Gap

The microstrip Yagi antenna is fed by the microstrip line, selected for its ease of fabrication, simple matching by controlling the inset position, and straightforward modeling. To optimize the feeding length, LF and LF1 are designed as $\lambda g/\sqrt{2}$ and $\lambda g/2$, respectively. As mentioned before, the design antenna is started with driven element and then it is accomplished by having the parasitic

elements in the forward beam act as directors while those in the rear act as reflectors. Figure 2.2 presents the parameters list of the dimensions of the two branch Yagi.

2.4 Triangle Microstrip Design

The triangle geometry, can be used as a microstrip form to emulate the response of a Yagi-Uda microstrip, avoiding reflectors and directors the response can be improved without the parasitic elements in the system. The triangular shape allows for efficient beamforming and radiation pattern control, which enhances the antenna's directivity and gain. Moreover, this design simplifies the fabrication process and reduces the overall complexity of the antenna system, making it a promising alternative for achieving Yagi-Uda-like performance in a microstrip configuration.

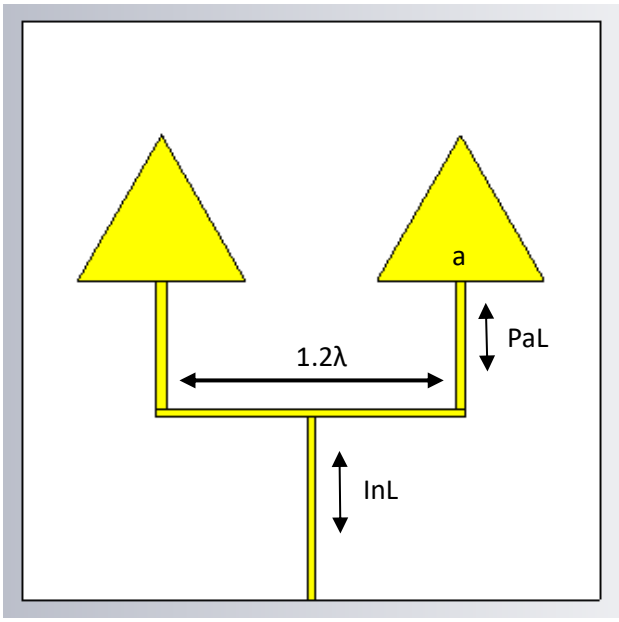

Figure 2.4 Triangular Microstrip Array.

Table 2.2 Triangle microstrip array dimensions.

Parameter	Value	Description
InL	Lg/sqrt(2)	Input link length
paL	Lg/2	Triangle link length
Total width and length	60	Substrate dimensions
Lg	26.7	Lambda g
a	17.4	Triangle sides lengths
b	1.2	Central link length Lg factor
InW	0.85	Input link width
h	0.9906	Substrate thickness
Cu	0.018	Cooper thickness

CHAPTER III

SIMULATION AND COMPARISON OF ANTENNA RESPONSE

Researchers and engineers may efficiently assess and optimize antenna designs by using electromagnetic computational software. An extensive analysis of alternative antenna topologies and their performance characteristics is made possible by the well-known electromagnetic modeling program CST Microwave Studio. CST Studio Suite® offers multiple electromagnetic (EM) simulation solvers which use methods such as the finite element method (FEM) the finite integration technique (FIT), and the transmission line matrix method (TLM). These represent the most powerful general-purpose solvers for high frequency simulation tasks. The software simulates, calculates, and provides essential antenna parameters, i.e., radiation patterns, gain, bandwidth, and impedance matching, etc. By simulating and comparing the responses of several antenna models under various conditions, such as various frequencies and polarizations, users are able to compare and optimize the antenna's performance. These tools enable scientists to choose the best antenna for a given application and make educated design decisions. The software's sophisticated visualization tools make it easier to analyze simulation findings and find potential design improvements. In the end, this procedure guarantees the development for a variety of wireless communication systems and applications, of high-performance antennas.

In addition to its simulation capabilities, CST software offers a powerful Optimization Toolbox that plays a crucial role in fine-tuning antenna designs. Based on specified goals and restrictions, the Optimization Toolbox uses sophisticated algorithms to automatically alter antenna characteristics and improve performance. The toolbox will iteratively explore the parameter space to identify the optimum configuration that satisfies desired goals, such as optimizing antenna gain, decreasing return loss, or creating a certain radiation pattern, when researchers provide desired goals. Compared to conventional trial-and-error procedures, this strategy can save a lot of time and effort. Additionally, the Optimization Toolbox enables simultaneous analysis of many design aspects, resulting in more thorough and effective optimizations. Antenna designers can create unique and extremely effective antenna solutions by utilizing this potent feature, improving the general performance and dependability of communication systems in a variety of real-world applications.

3.1 Rectangular and Triangular Array Response Comparison

We compare the antenna responses for two alternative designs, rectangular and triangular arrays in this section. The S_{11} reflection coefficient of the rectangular array, which works at 5.7 GHz, is -26 dB, demonstrating satisfactory impedance matching. In the polar plot, it has a gain of 8.548 dBi and a beamwidth of 55.5 degrees. On the other hand, the Triangular array has an S_{11} value of -25.5 dB and runs at a little lower frequency of 5.63 GHz. It exhibits a smaller beamwidth of 47.2 degrees and a gain of 8.39 dBi. Both designs have been proposed using the Arlon DiClad 880 folding substrate, which improves their performance qualities. The comparison offers insightful information about the trade-offs between these two antenna arrangements, allowing for

a well-informed choice based on the requirements of the application. A study comparison is conducted between different designs and responses are shown in table 3.1.

Table 3.1 Rectangular and triangle array response

Pattern Design	Radiation Pattern	Polar	Performance
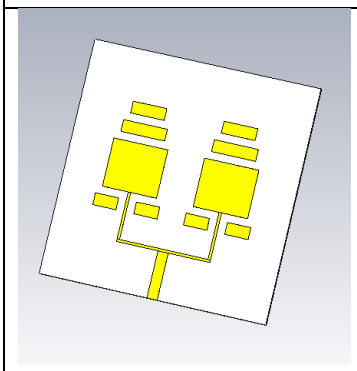	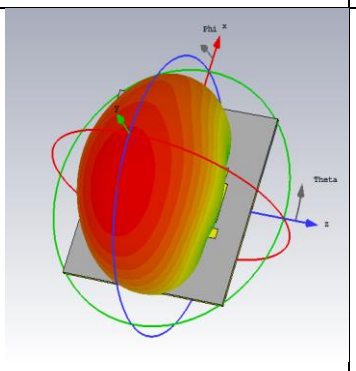	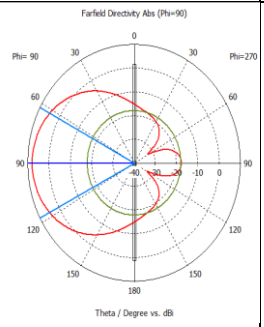	fc = 5.7 GHz S_{11} = -26 dB Gain= 8.54 dBi Angular Width, 3 dB (AW) = 55.5 °.
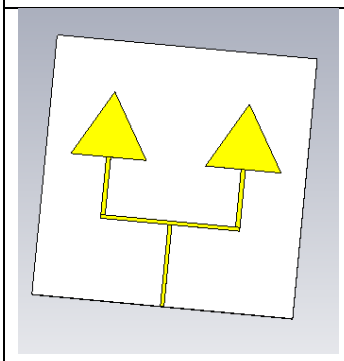	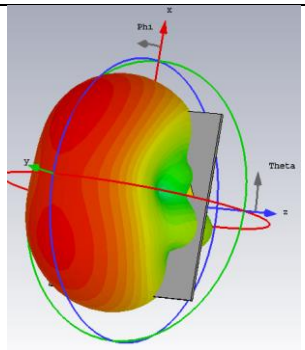	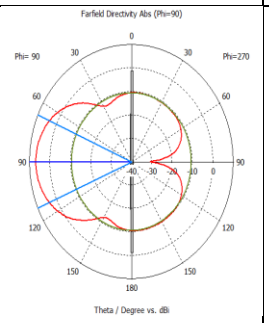	fc = 5.63 GHz S_{11}: -25.5 Gain 8.39 dBi AW: 47.2 °

3.2 1st Approach: Single Plane Folded Patch

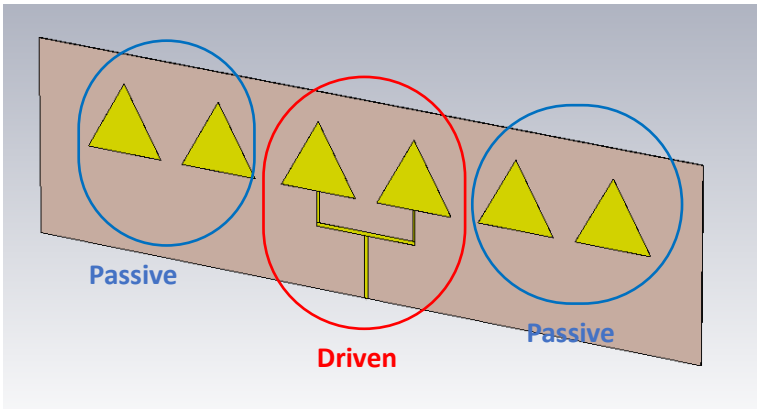

Figure 3.1 1st Approach: Single-plane folded patch CST design.

The analysis of the triangular array was mentioned in Chapter 2.1 using design criteria. Four more directors have been added to examine how they affect antenna response. On either side of the driven elements are these passive directors. To get the best antenna performance, the design parameters have been improved by utilizing the Optimization Toolbox in the CST software. This tool can be used to specify optimization goals, such as maximizing gain, minimizing return loss (S_{11}), or producing a specific radiation pattern. The toolbox then methodically searches the parameter space, iteratively changing the directors' sizes and positions to find the optimal arrangement that achieves the desired goals.

By tweaking the design parameters, this optimization method permits the improvement of antenna performance. It guarantees that the antenna performs with better impedance matching and radiation characteristics at the intended frequency. Gain, beamwidth, and other important aspects of the antenna can be greatly enhanced by the optimal design, leading to an antenna that more effectively satisfies the demands of the intended application. Thus, using CST's Optimization Toolbox makes it easier to create a high-performance antenna design with increased efficacy. In figure 3.1 the final design is shown.

At a frequency of 5.818 GHz, the far-field study exposes important details regarding the antenna's radiating properties and general effectiveness. The antenna's gain with respect to an isotropic radiator is shown by the "Directivity" measurement, which yields information about how well it can concentrate and direct the emitted energy. This measurement is 10.36 dBi. The "Radiation Efficiency" of 2.257 dB measures the antenna's efficiency in converting input power into electromagnetic waves that are radiated, and the "Total Efficiency" of -2.459 dB accounts for all losses in the antenna system, including radiation, conductor losses, and dielectric losses.

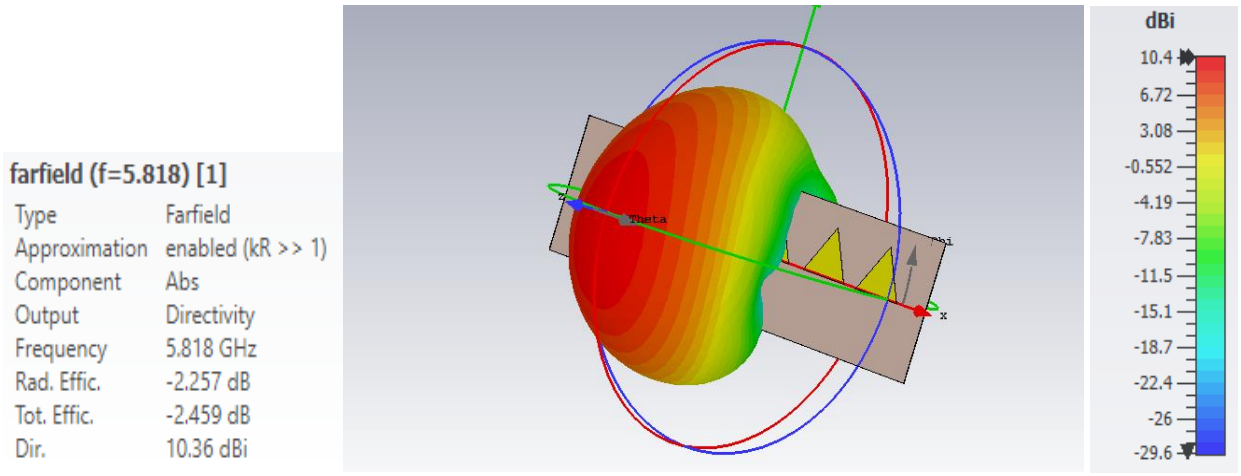

Figure 3.2 1st Approach: Single plane folded patch far-field response.

The S_{11} response of the antenna is shown below, with a -20 dB at 5.8 GHz.

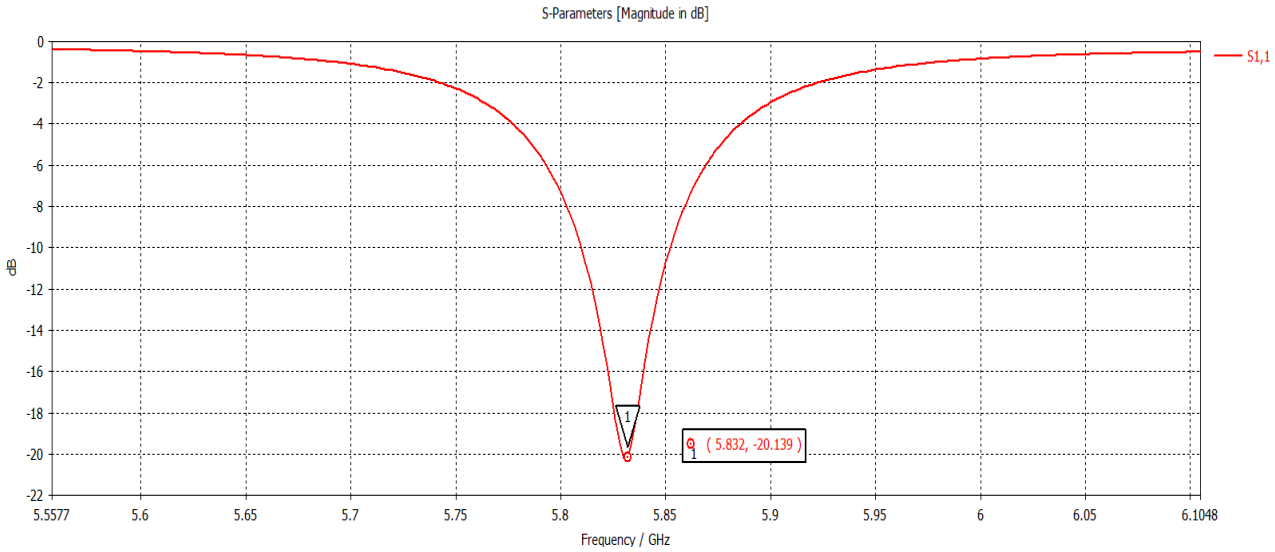

Figure 3.3 1st Approach: Single-plane folded patch S11 response.

3.3 1st Approach: Single-Plane Folded Patch Antenna Study

The primary objective of this work is to investigate the folding of antenna substrates in four different scenarios: one side with just passive elements, two sides with passive elements, one side with a folding microstrip line of active elements, and two sides with a folding microstrip line

of active elements. Analysis of the antenna response at different folding angles, specifically 15, 30, 45, 60, and 75 degrees, is the main goal. Important factors like the reflection coefficient (S_{11}), directivity, beam pattern, and frequency are all considered in the analysis. This thorough analysis offers insightful information on how various folding arrangements affect the performance of the antenna. These results are crucial for improving antenna design and ensuring that the final configuration complies with the specifications of various real-world applications.

3.3.1 One Side Unfolded Microstrip Line Simulation Response

This first case is focused when substrate is only folding passive elements without folding microstrip line. The table 3.2 shows the results of a simulation study for antenna response at various folding angles, 15°, 30°, 45°, 60°, and 75°. 3D farfield response are shown in the table. A certain operating frequency, S_{11} reflection coefficient, gain, and beamwidth are matched to each folding angle.

The antenna operates at 5.822 GHz with an S_{11} value of -19.43 dB at a folding angle of 15°, displaying a respectable impedance match. The beamwidth is 45.6°, and the gain is 8.019 dBi. The operational frequency is 5.806 GHz, and the S_{11} value is -19.532 dB for a folding angle of 30°. The antenna has a gain of 8.24 dBi and a 43-degree beamwidth. The antenna operates at 5.8 GHz with an S_{11} value of -18.745 dB at a folding angle of 45°. The beamwidth is 40.7 degrees, and the gain is 8.515 dBi. The operational frequency is 5.828 GHz, and the S_{11} value is -19.189 dB for a folding angle of 60°. The antenna has an 8.776 dB gain and a 36.7° beamwidth. Finally, the antenna functions at 5.844 GHz with an S_{11} value of -20.046 dB at a folding angle of 75°. The beamwidth is 36.6 degrees, and the gain is 8.7 dBi.

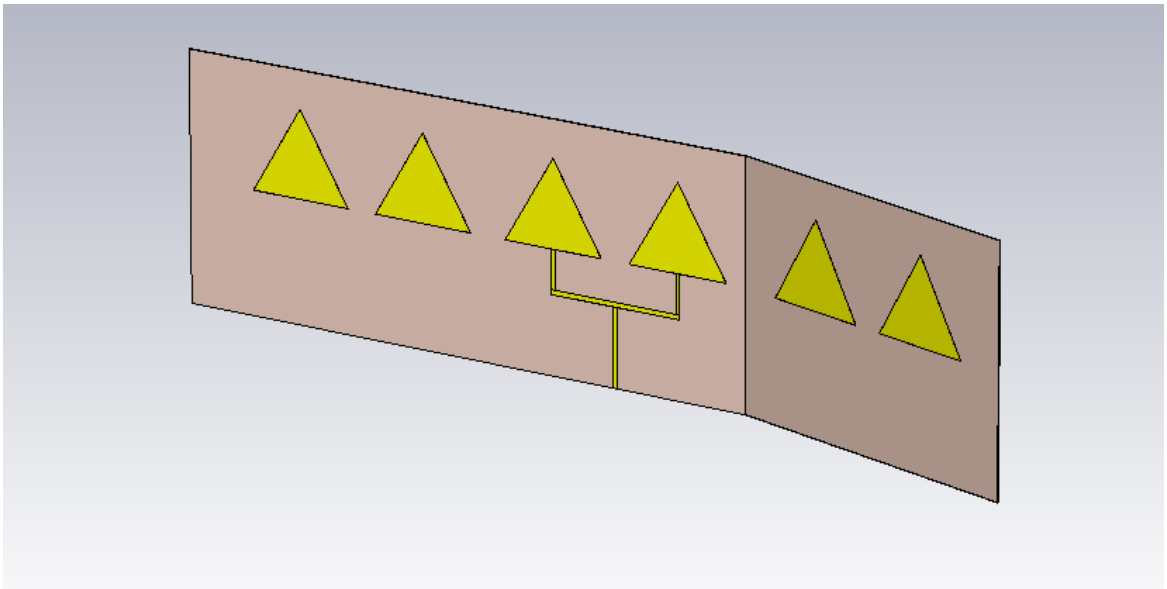

Figure 3.4 1st Approach: Single-plane folded patch one side at 15°.

Table 3.2 1st Approach: single-plane, single-side folded patch study.

Angle	Radiation Pattern	Polar Plot	Performance
15°	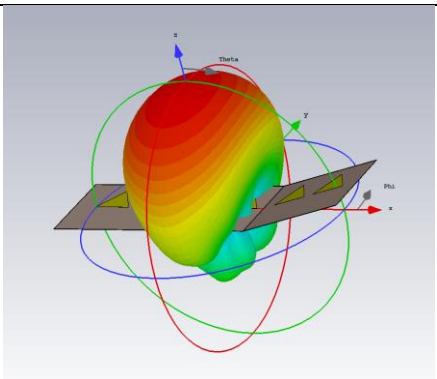	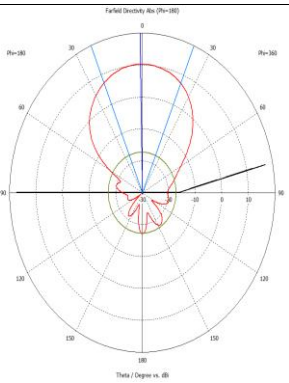	f_c =5.822 GHz. S_{11}= -19.43 Gain = 8.019 dBi. AW = 45.6°
30°	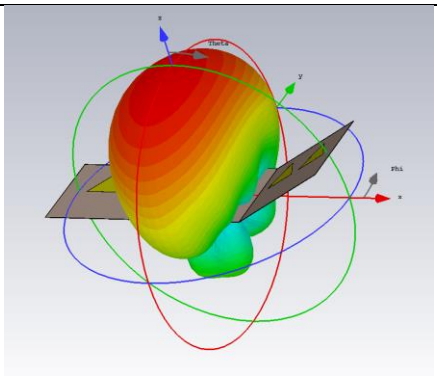	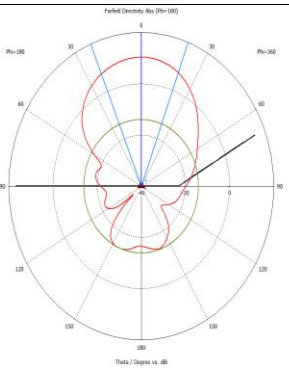	f_c = 5.806 GHz S_{11}: -19.532 Gain = 8.24 dBi. AW= 43°

Table 3.2., Cont.

45°	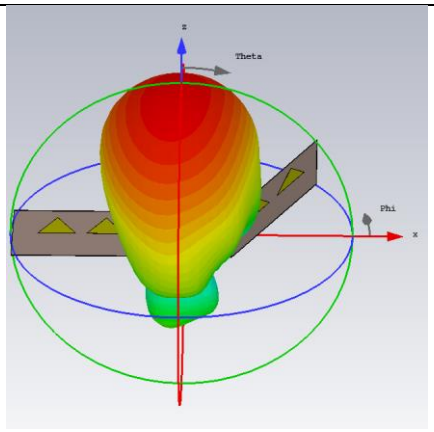	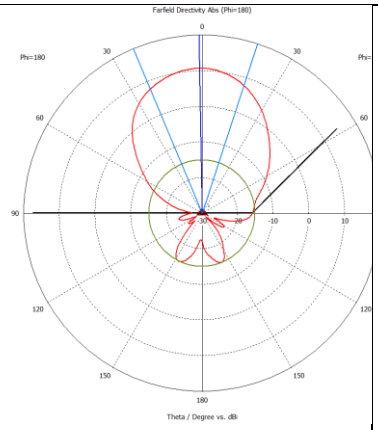	f_c = 5.83 GHz S_{11}=-18.745 Gain = 8.515 dBi. AW= 40.7°
60°	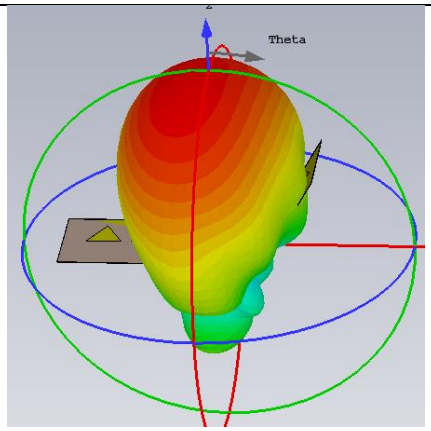	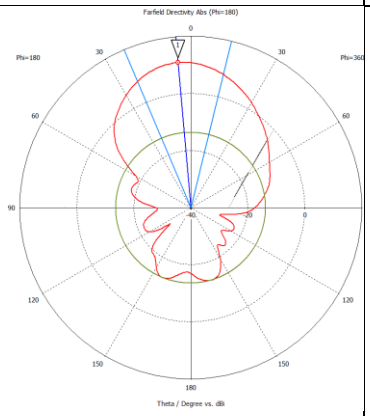	f_c =5.828 GHz S_{11}=-19.189 Gain = 8.776 dBi. AW=36.7°
75°	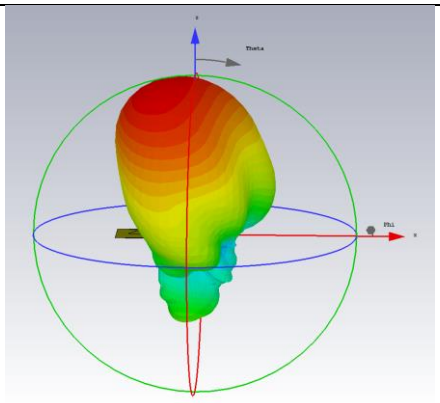	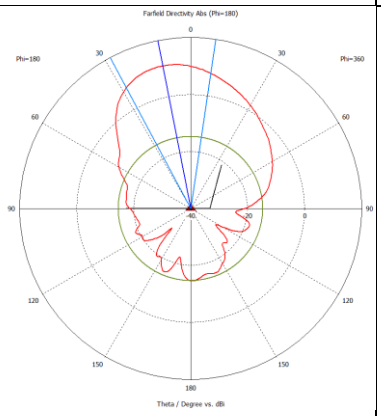	f_c =5.844 GHz. S_{11}=-20.046 Gain = 8.7 dBi AW= 36.6 °

Following the S_{11} parameters comparison chart. We can see that frequency shifts when substrate folds from 5.8 GHz to 5.85 GHz. And S_{11}-parameters response seems to be not affected by folding passive elements.

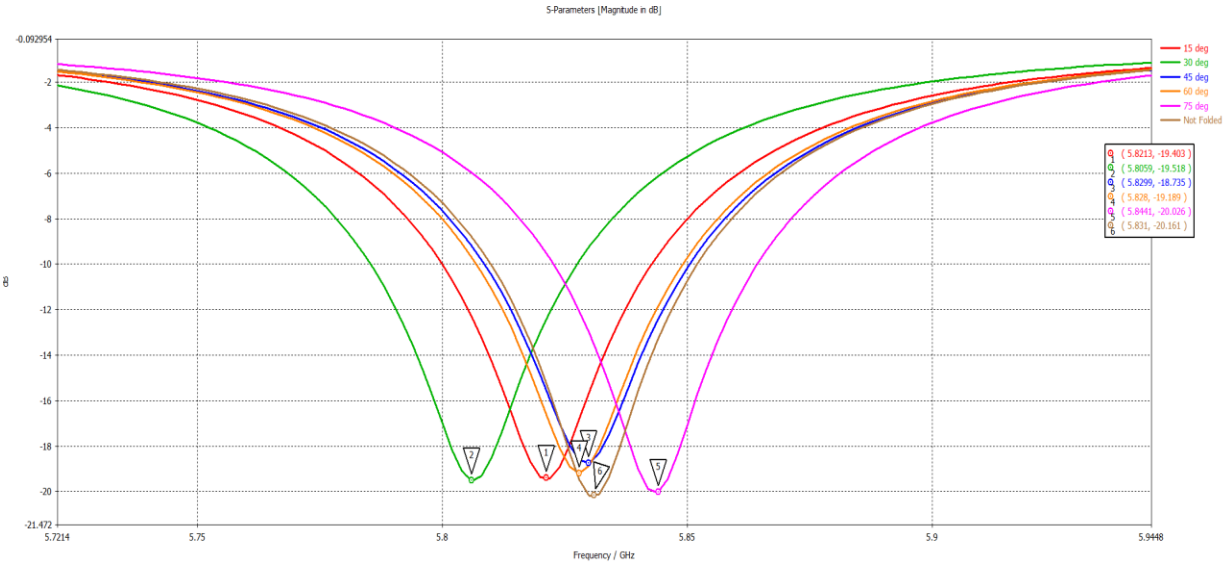

Figure 3.5 S_{11} parameters of one side folded without folding microstrip line.

3.3.2 Two Sides Unfolded Microstrip Line Simulation Response

The simulation response displays the findings of an investigation into the behavior of antennas when a substrate is folded on both sides using solely passive components, without folding the microstrip line. The analysis is carried out for different folding angles, including 15°, 30°, 45°, 60°, and 75°. A distinct operating frequency, S_{11} reflection coefficient, and directivity (in dBi) are associated with each angle.

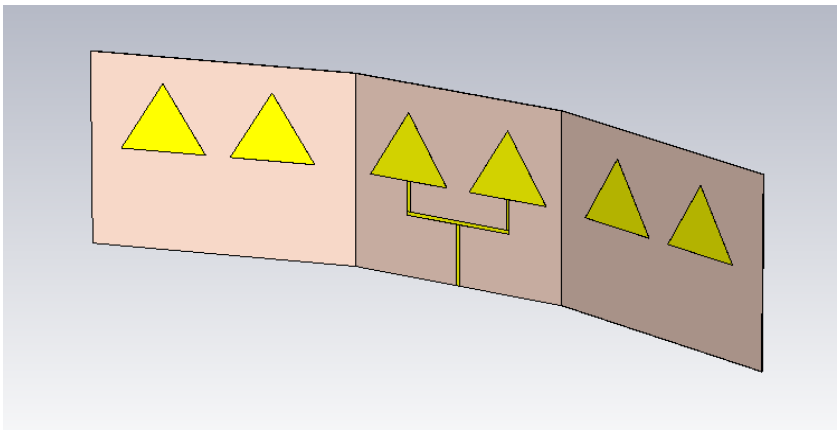

Figure 3.6 1st Approach: Single-plane folded patch, two side folded at 15°.

Table 3.3 1st Approach: single-plane, double-side folded patch response.

Angle	Radiation Pattern	Polar Plot	Performance
15°	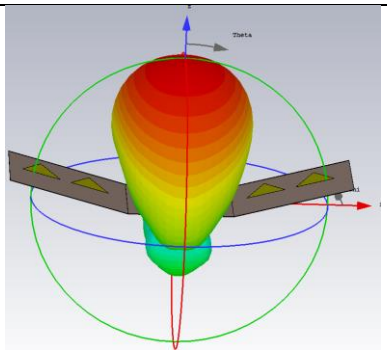	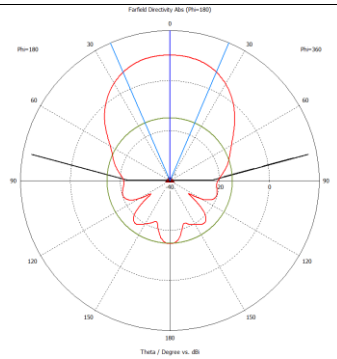	f_c =5.828 GHz $S_{11=}$ -18.968 Dir= 10.28 dBi
30°	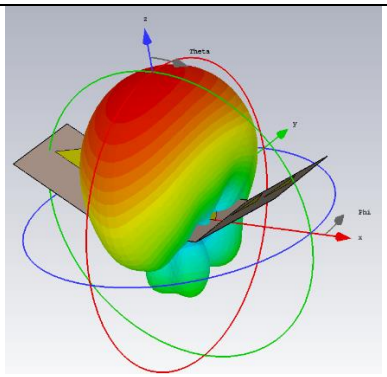	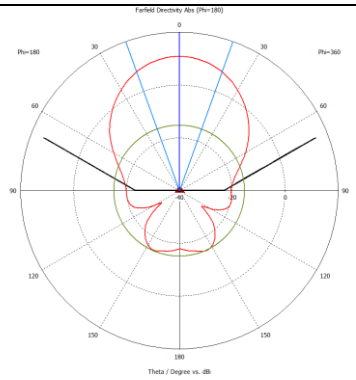	f_c =5.828 GHz S_{11} =-19.583 Dir. =10.95 dBi
45°	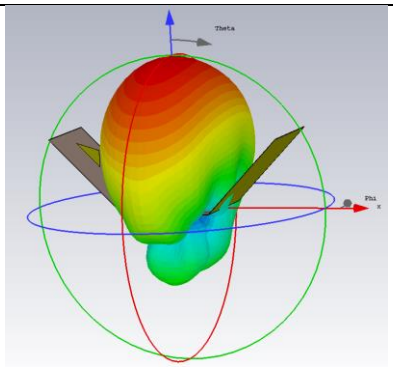	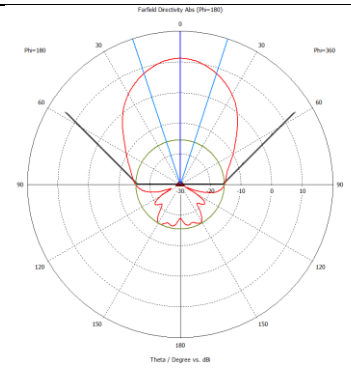	f_c =5.834 GHz S_{11} =-19.22 Dir=. 11.33 dBi
60°	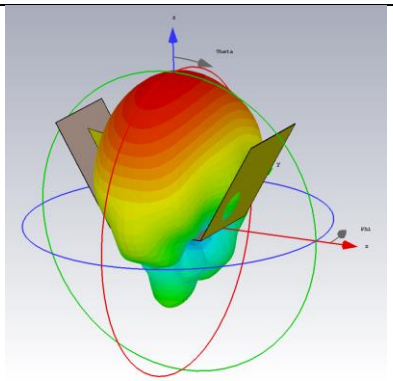	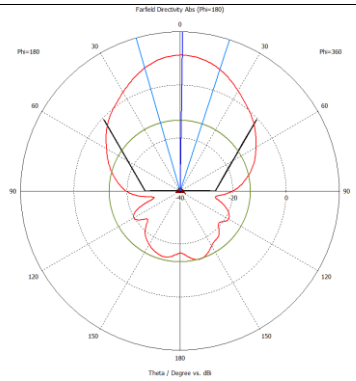	f_c =5.8193 GHz S_{11} =-19.016 Dir. =11.28 dBi

Table 3.3., Cont.

75°	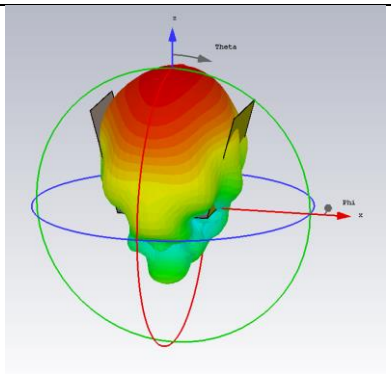	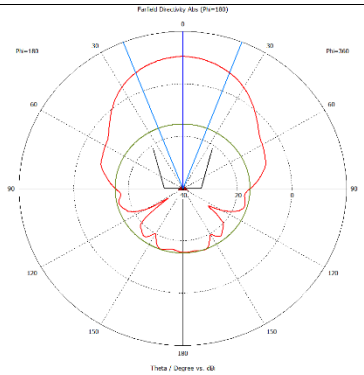	f_c =5.8364 GHz S_{11} = -19.157 Dir.= 10.48 dBi

The antenna operates at 5.828 GHz with an S_{11} value of -18.968 dB at a folding angle of 15°, showing a good impedance match. 10.28 dBi is the directivity measurement. The operational frequency remains at 5.828 GHz for a folding angle of 30°, and the S_{11} value is -19.583 dB. 10.95 dBi is the increase in directivity. The antenna operates at 5.834 GHz with an S_{11} value of -19.22 dB at a 45° folding angle. Directivity is now 11.33 dBi, which is an improvement. With an S_{11} value of -19.016 dB and an operating frequency of 5.8193 GHz at a folding angle of 60°. 11.28 dBi is the directivity measurement. Finally, the antenna operates at 5.8364 GHz with an S_{11} value of -19.157 dB at a folding angle of 75°. 10.48 dBi of directivity were attained. One side – When Substrate is folding microstrip line of active elements.

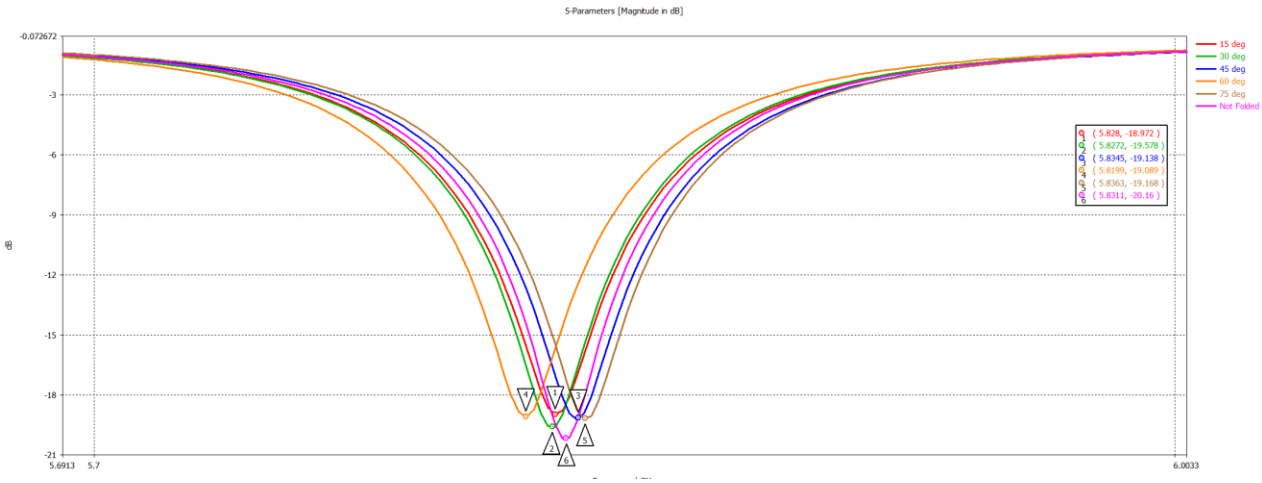

Figure 3.7 S11 parameters of two side folded with folding microstrip line.

3.3.3 One Side with Folded Microstrip Line Simulation Response.

The simulation response sheds light on how well the antenna performs when the microstrip line is folded into one side of the substrate. The antenna's behavior is investigated at folding angles of 15, 30, 45, 60, and 75 degrees. Specific operating frequencies, S_{11} reflection coefficients, and directivity (in dBi) are connected to each angle.

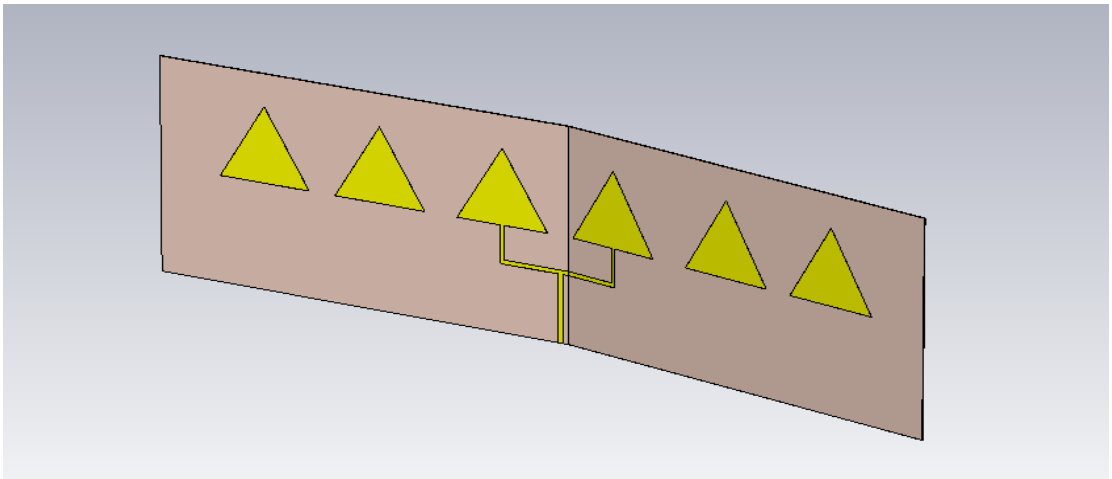

Figure 3.8 1st Approach: Single-plane folded patch, one side folding with microstrip line at 15°.

Table of simulations is presented below.

Table 3.4 Single-side folded microstrip line simulation response.

Angle	Radiation Pattern	Polar Plot	Performance
15°	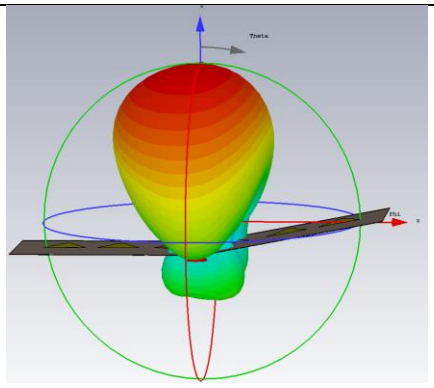	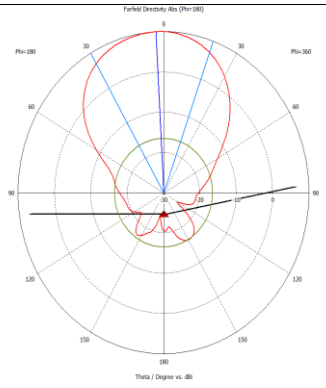	f_c =5.8402 GHz S_{11} =-18.709 Dir= 10.08 dBi

Table 3.4., Cont.

30°	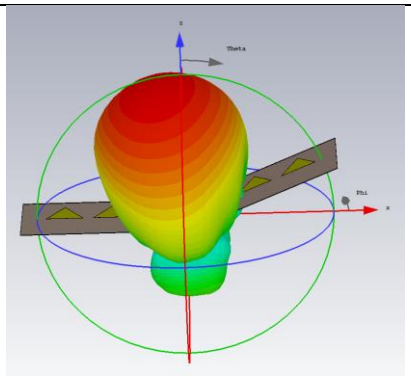	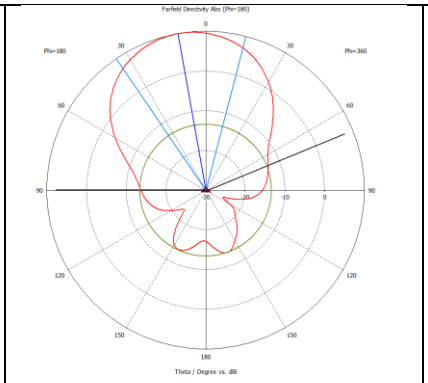	f_c =5.822 GHz S_{11} =-21.952 Dir= 10.12 dBi
45°	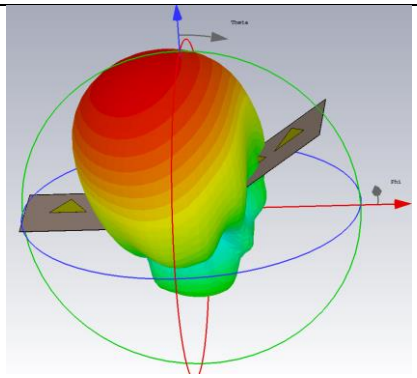	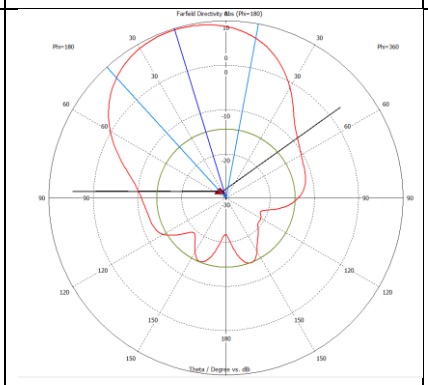	f_c =5.8301 GHz S_{11}=-23.897 Dir= 9.969 dBi
60°	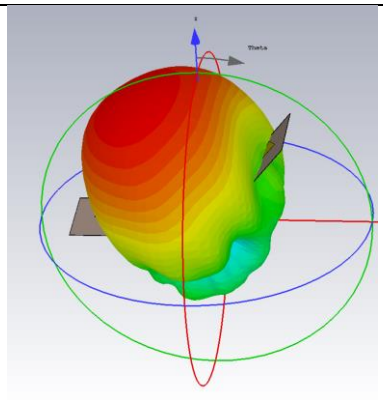	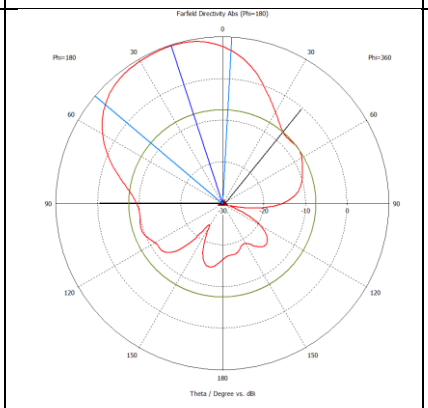	f_c =5.83 GHz S_{11}= -26.648 Dir= 10.13 dBi
75°	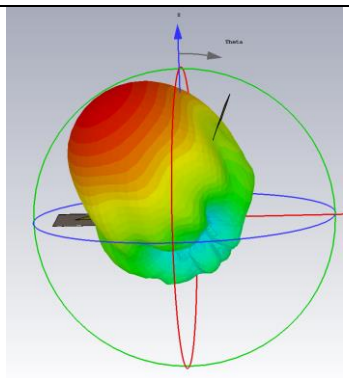	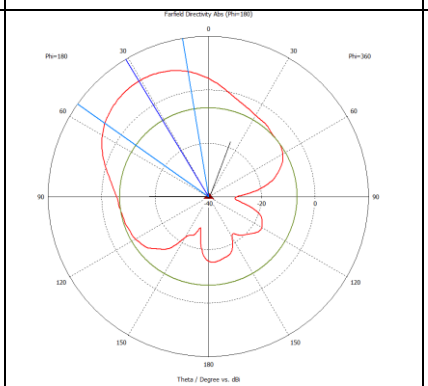	f_c =5.8404 GHz S_{11}=-22.472 Dir =10.79 dBi

Following the S_{11} parameters comparison graphic. We can see that frequency shift when substrate folds from 5.82 GHz to 5.84 GHz. And S_{11}-parameters response is affected by folding microstrip elements.

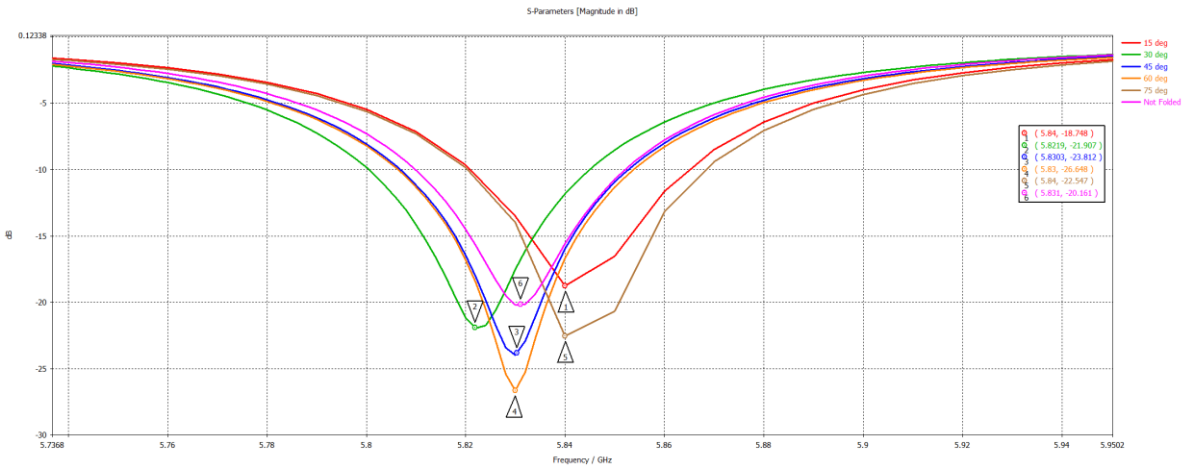

Figure 3.9 S_{11} parameters of one side with folding microstrip line.

3.3.4 Two Sides with Folded Microstrip Line Simulation Response.

The simulation study investigates the antenna response when the substrate is folded on both sides, using the folding of active microstrip lines. The investigation looks at how the antenna behaves at folding angles of 15, 30, 45, 60, and 75 degrees. Results for the S_{11} reflection coefficient, directivity (in dBi), and relevant operating frequencies are included in the data.

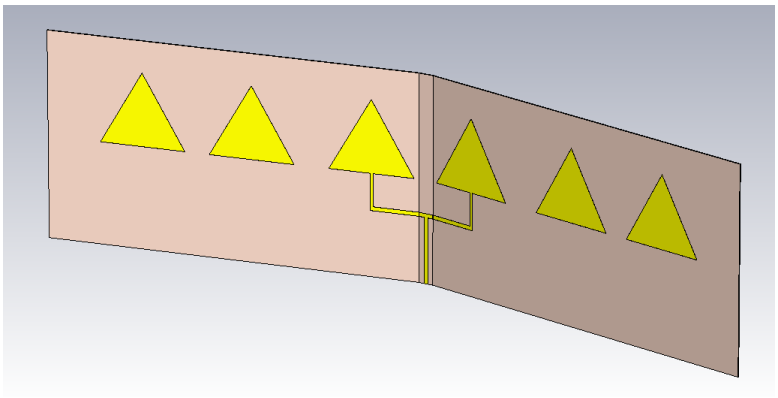

Figure 3.10 1st Approach: Single-plane, two side folding with microstrip line at 15°.

The antenna operates at 5.824 GHz with an S_{11} value of -21.892 dB at a folding angle of 15°, demonstrating a suitable impedance match. 9.748 dBi is the directivity measurement. The operational frequency is 5.83 GHz and the S_{11} value is -25.678 dB for a folding angle of 30°. A value of 9.98 dBi is achieved for the directivity. The antenna operates at 5.804 GHz with an S_{11} value of -30.238 dB at a 45° folding angle. To 11.12 dBi, the directivity dramatically increases. The working frequency for a folding angle of 60° is 5.818 GHz, and the S_{11} value is -17.385 dB. 12.37 dBi of directivity are achieved. Finally, the antenna runs at 5.8258 GHz with an S_{11} value of -6.9285 at a folding angle of 75°. The simulation results of farfield and polar response are shown in the table below.

Table 3.5 Double-side folded microstrip line simulation response.

Angle	Radiation Pattern	Polar Plot	Performance
15°	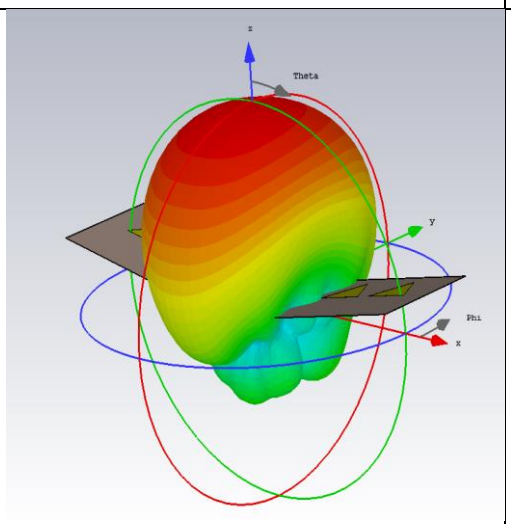	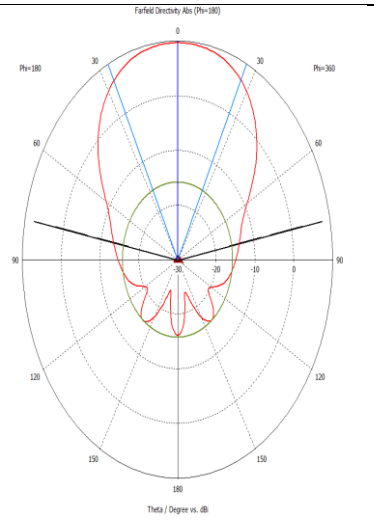	f_c =5.824 GHz S_{11}= -21.892 Dir= 9.748 dBi

Table 3.5., Cont.

30°	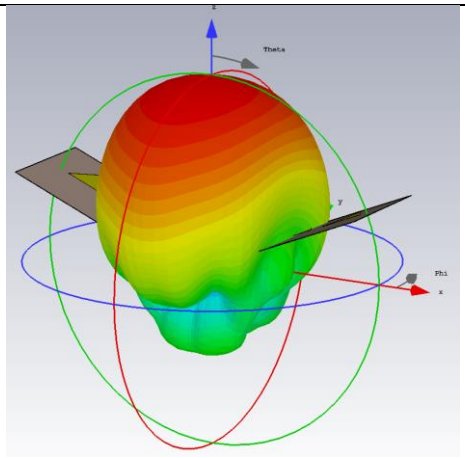	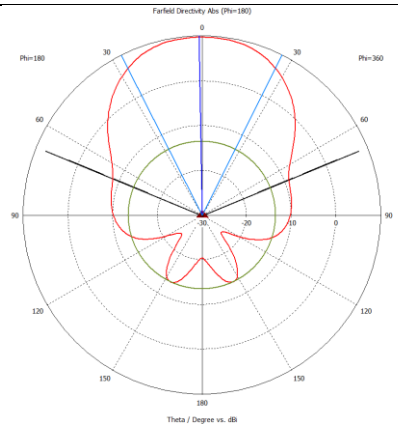	f_c =5.83 GHz S_{11}=-25.678 Dir=9.98 dBi
45°	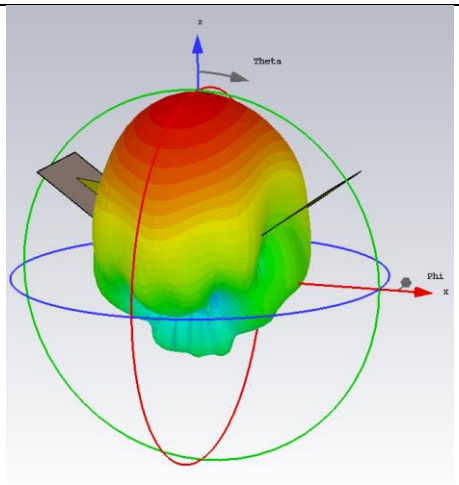	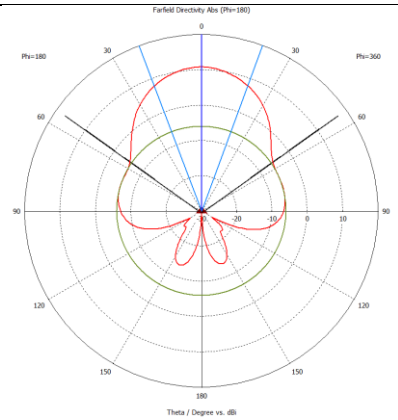	f_c =5.804 GHz S_{11}=-30.238 Dir= 11.12dBi
60°	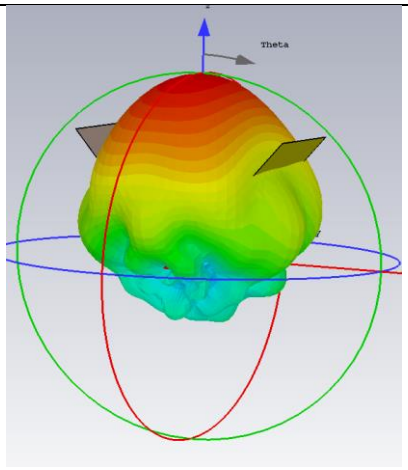	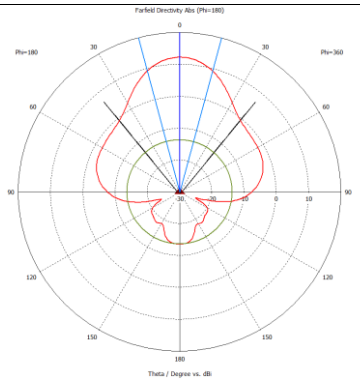	f_c =5.818 GHz S_{11}= -17.385 Dir= 12.37 dBi

Table 3.5., Cont.

75°	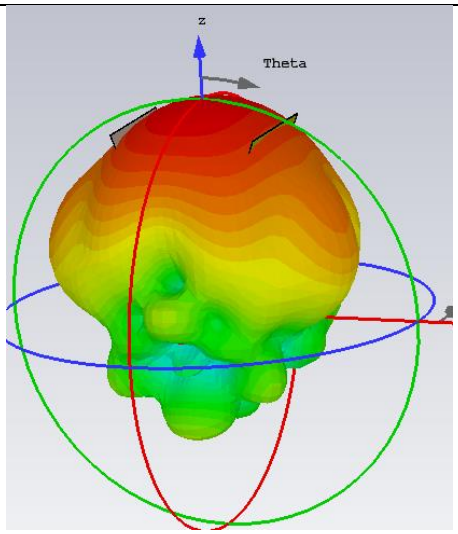	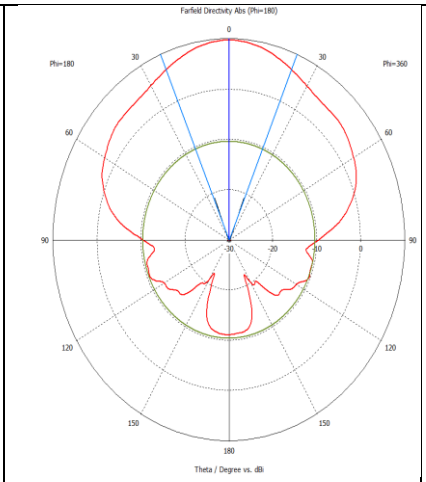	f_c =5.8258 GHz S_{11}=-6.9285 Dir= 9.696 dBi

S_{11} parameters of both sides folded, with microstrip line:

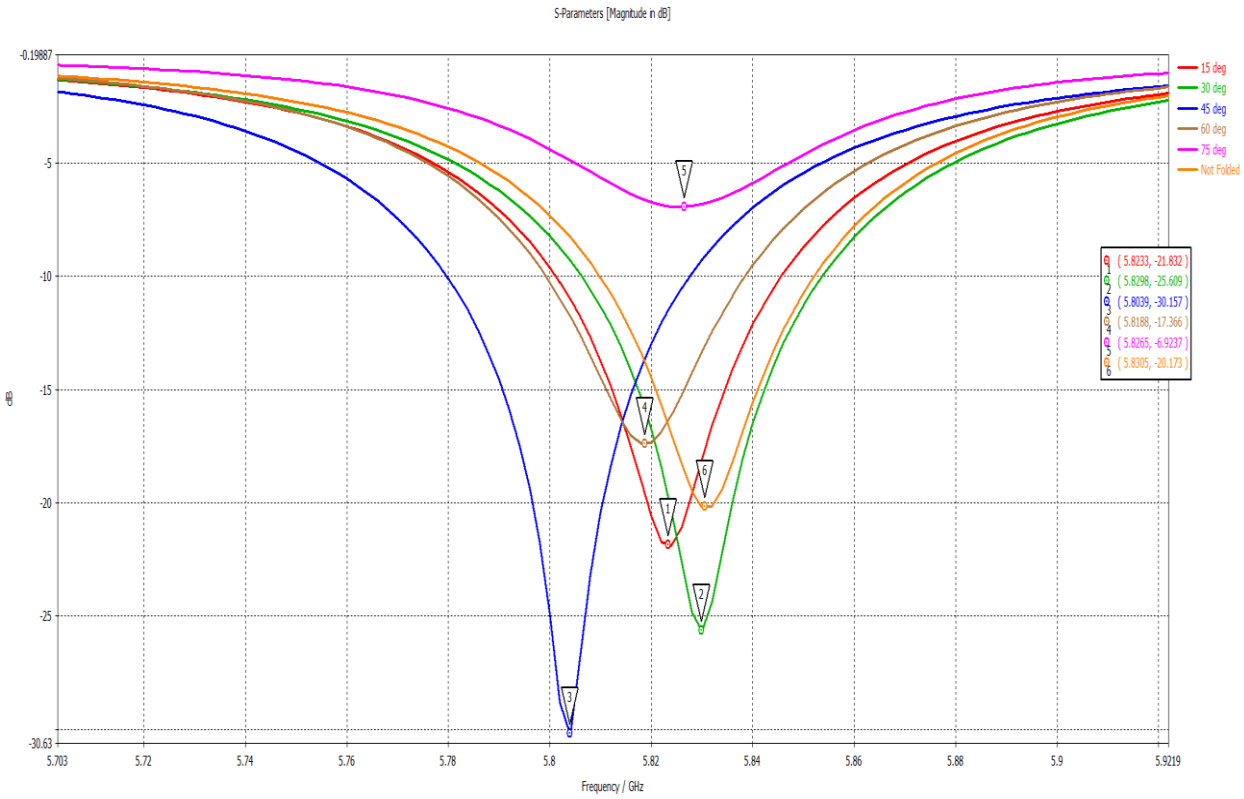

Figure 3.11 S_{11} response of double-side folded microstrip line.

3.3.5 Curvature Folded Substrate

The use of a curvature folding substrate in antenna design has special benefits, such as increased beam directionality and radiation patterns. In situations where a high-gain and well-directed radiation pattern is required, such designs are very advantageous. This thesis presents this idea just as proof of concept of the different geometries than can be achieved. Looking to optimize circular folding substrate designs for various wireless communication systems and associated applications, this simulation result is extremely helpful.

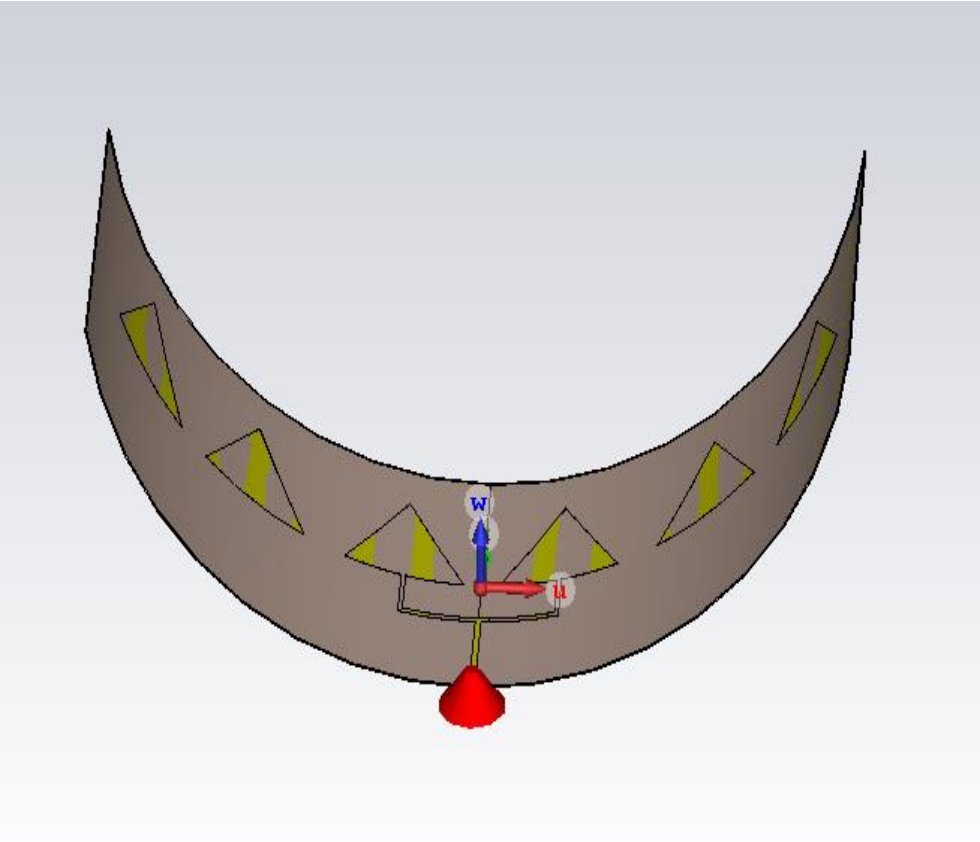

Figure 3.12 Semicircular folding 1st Approach: Single-plane folded patch.

Create efficient and effective antenna solutions by utilizing these insights, thus improving the overall performance and dependability of communication systems can be helpful for specific applications.

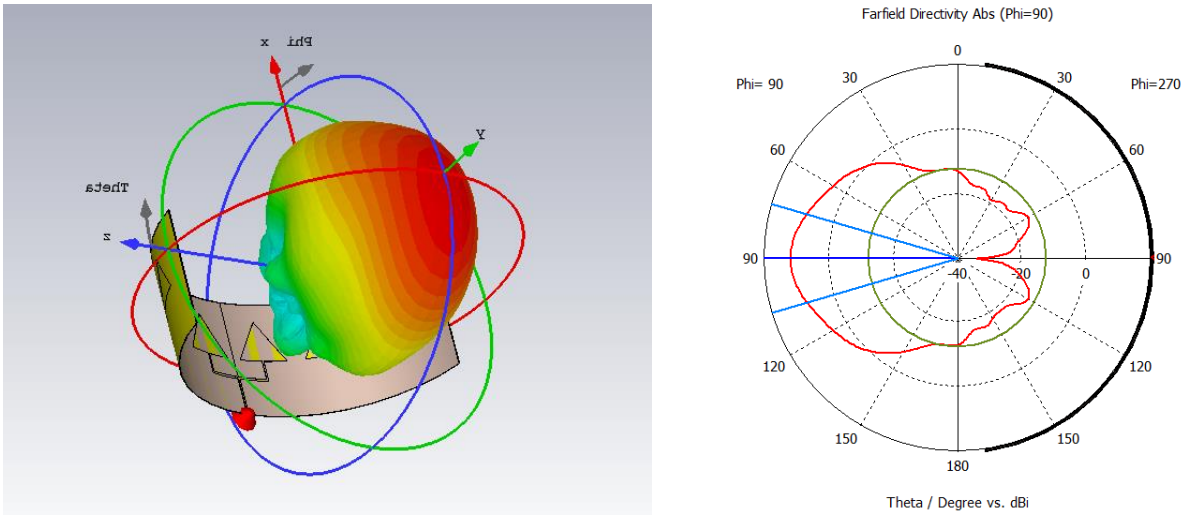

Figure 3.13 1st Approach: Single-plane semicircular folding far-field and polar response.

The antenna response is shown in the simulation of the circular folding substrate at 5.819 GHz, which is its operational frequency. A good impedance match is shown by the S_{11} value, which measures the reflection coefficient and is recorded at -18.57 dB. The antenna's capacity to efficiently focus and direct the radiated energy is demonstrated by the directivity achieved, which is 11.86 dBi.

3.4. 2nd Approach: Double-Plane Patch

We concentrate on a four-element antenna array design in section 3.4 where the directors are parallel to the driven elements' plane. The radiation pattern and overall performance of the antenna are significantly shaped by the array design, which is a crucial component in antenna engineering.

The driven element, which is the primary radiating element in the four-element antenna array, and the directors, which are passive devices positioned next to the driven element, are among

the antenna elements that make up the array. These directors are essential for improving the radiation in the desired direction and raising the gain and directivity of the antenna.

The simulation research of the four-element antenna array with directors parallel to the driven elements plane are covered in this section. This attempt aims to optimize the design by evaluating the antenna's response and radiation properties under various operating situations to get useful insights into the array's performance. This knowledge aids in the creation of high-performance antenna arrays appropriate for numerous communication applications, such as satellite communication, radar systems, and wireless communication systems, among others.

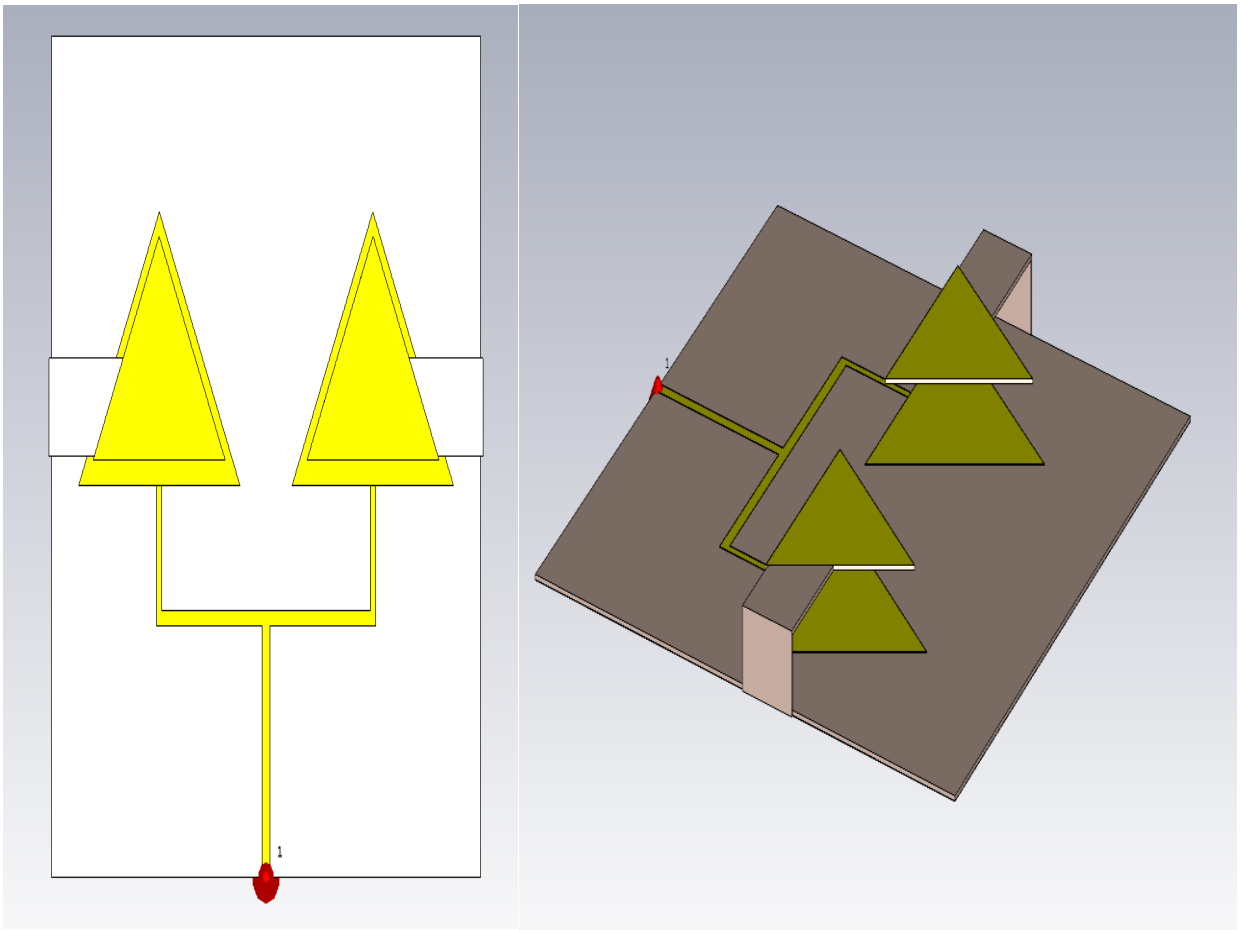

Figure 3.14 2nd Approach: Double-plane patch, directors parallel to the plane of driven elements.

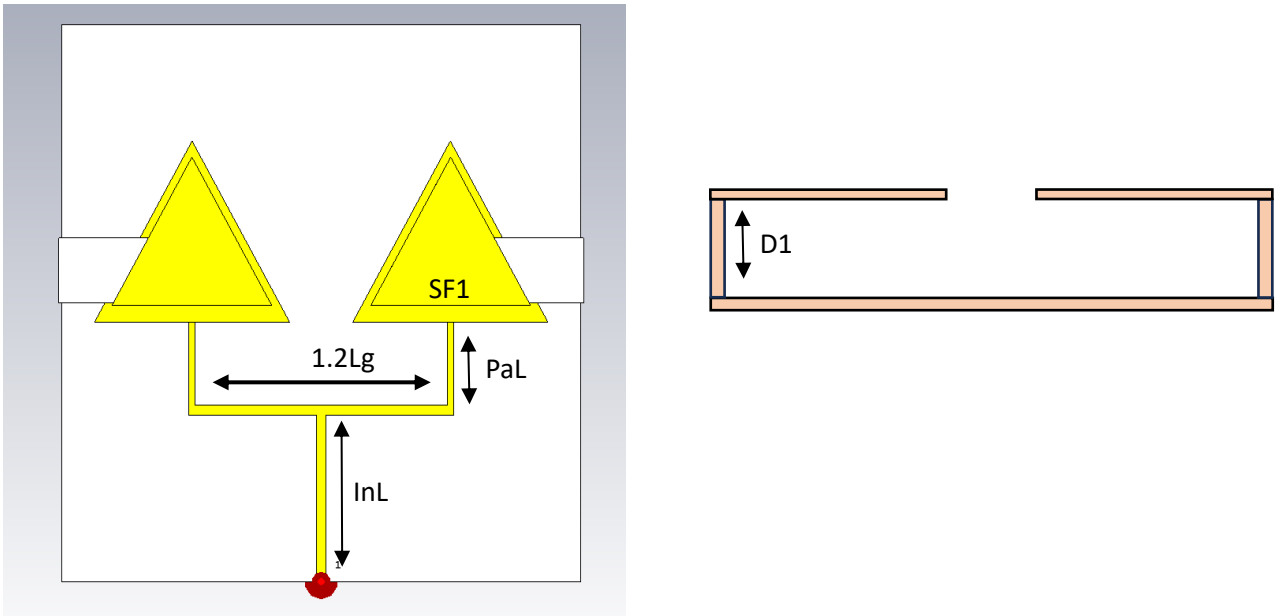

Figure 3.15 2nd Approach: Double-plane patch, design dimensions.

Table 3.6 2nd Approach: Double-plane patch, design dimensions.

Parameter	Value	Description
InL	Lg/sqrt(2)	Input link length
paL	Lg/2	Triangle link length
Lg	26.7	Lambda g
a	17.4	Triangle sides lengths
D1	3.77	Directors separation

S_{11} Response for the antenna design is shown above.

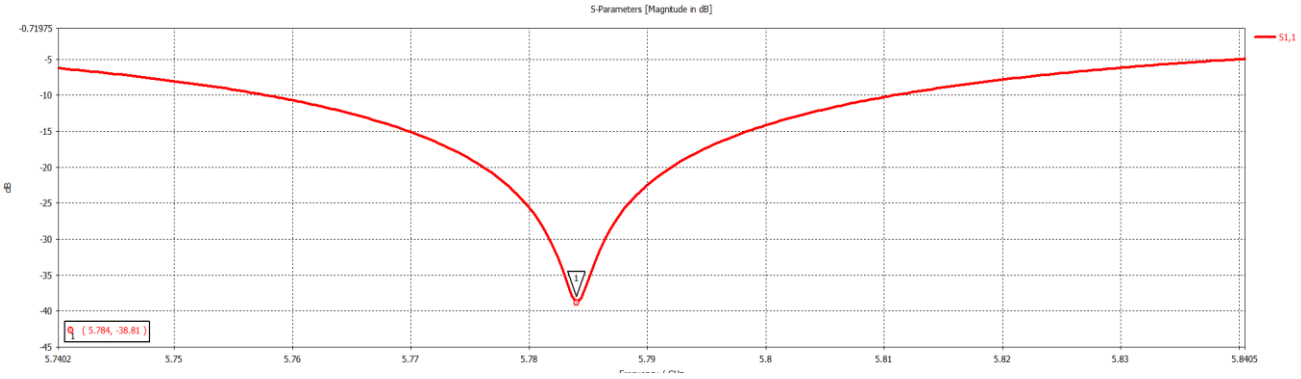

Figure 3.16 S11 2nd Approach: Double-plane patch response.

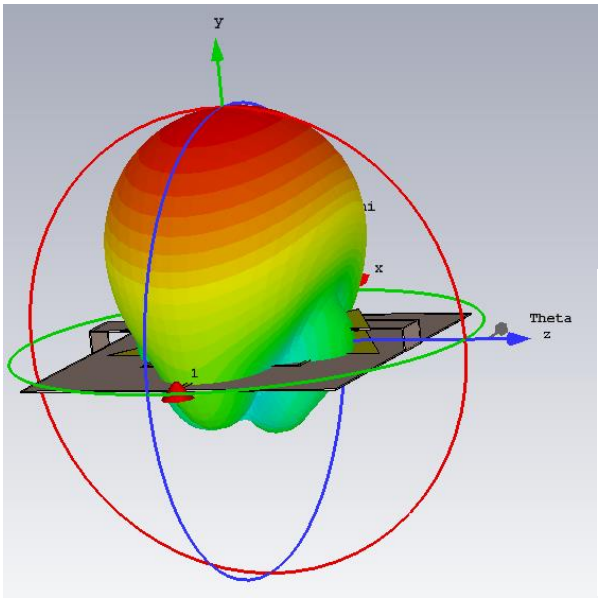

farfield (f=5.784) [1]

Type	Farfield
Approximation	enabled (kR >> 1)
Component	Abs
Output	Gain
Frequency	5.784 GHz
Rad. Effic.	-1.541 dB
Tot. Effic.	-1.542 dB
Gain	9.011 dBi

Figure 3.17 Far-field of 2nd Approach: Double-plane patch response.

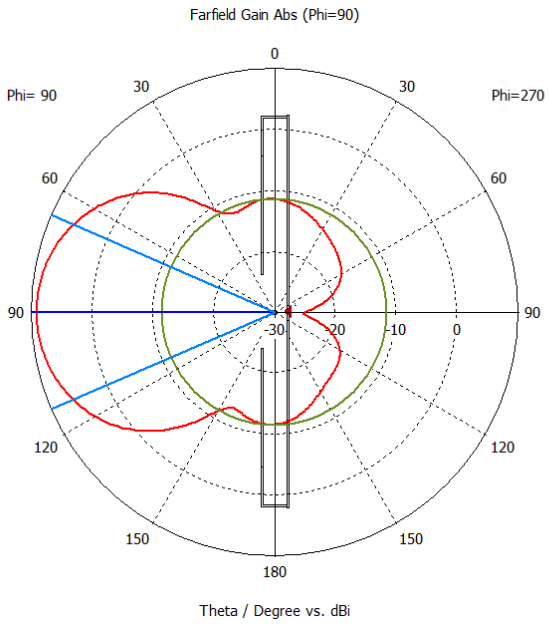

Frequency = 5.784 GHz
Main lobe magnitude = 9.01 dBi
Main lobe direction = 90.0 deg.
Angular width (3 dB) = 46.9 deg.
Side lobe level = -20.4 dB

Figure 3.18 Polar chart of 2nd Approach: Double-plane patch response.

The far-field radiation pattern or characteristics of the four-element antenna array are shown in Figure 3.17. A polar plot, shown in Figure 3.18, depicts the four-element antenna array's radiation pattern in polar coordinates.

3.4.1 Single-Folded Director Study Response

Through the adjustment of one director element at various angles, the study is investigating how a directional antenna responds. The experimental situations involved folding the antenna's one side at various angles, including 15, 30, 45, 60, 75, and 90 degrees. This study aims to evaluate the effects of the director's position changes on the radiation pattern and operation of the antenna. To accomplish this, rigorous observation, and analysis of the exact antenna measuring techniques.

Table 3.7 2nd Approach: Double-plane single director folded patch simulation response.

Angle	Radiation Pattern	Polar Plot	Performance
15°	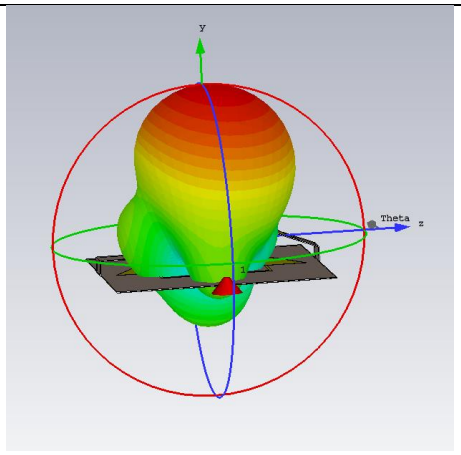	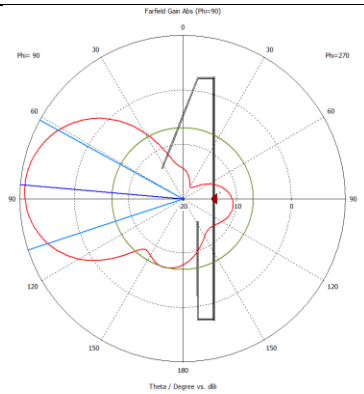	f_c = 5.7704 GHz. S_{11} = -45.237 Dir. = 9.14 dBi. AW = 47 Deg. SLL = -16.1 dB MLD = 85 °
30°	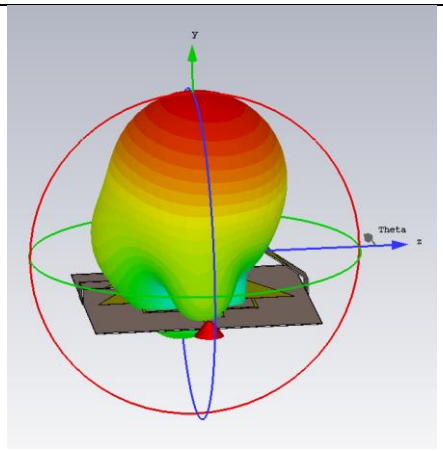	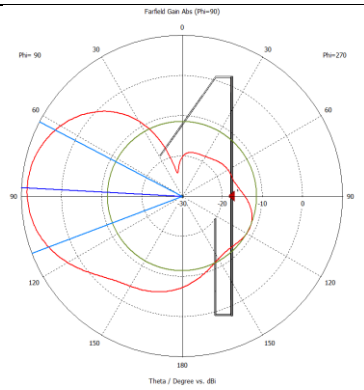	f_c =5.762 GHz S_{11} = -31.171 Dir = 8.54 dBi. AW = 48.4 Deg SLL = -20 dB MLD = 87 Deg

Table 3.7., Cont.

45°	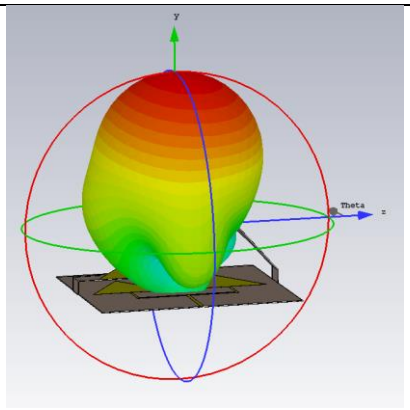	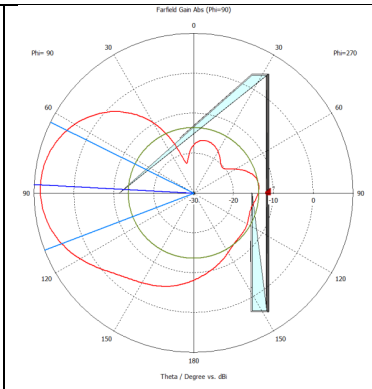	f_c = 5.7872 GHz S_{11} = -23.13 Dir = 8.37 dBi. AW = 47.4 Deg SLL = -21.9 dB MLD = 87 Deg
60°	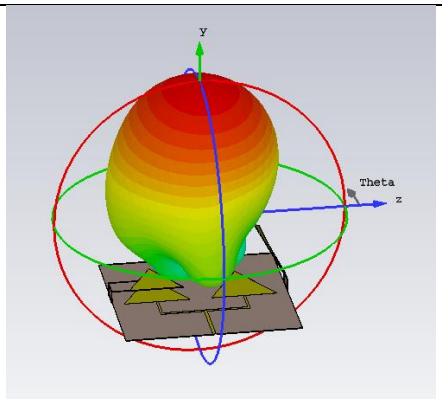	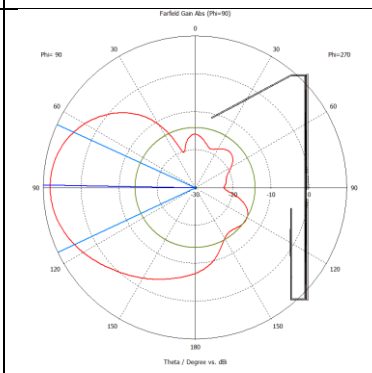	f_c = 5.7724 GHz S_{11} = -25.901 Dir = 8.16 dBi. AW = 49.9 Deg SLL = -22.3 dB MLD = 89 Deg
75°	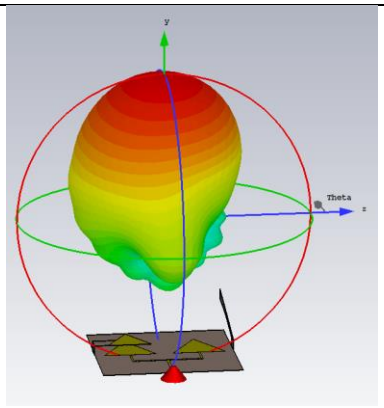	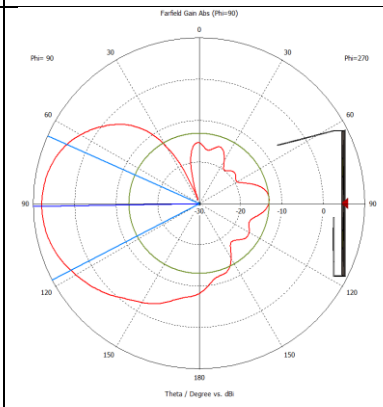	f_c = 5.7752 GHz S_{11} = -25.253 Dir = 7.9 dBi. AW = 51.6 Deg SLL = -21 dB MLD = 91 Deg
90°	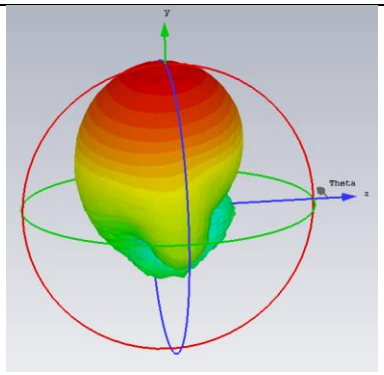	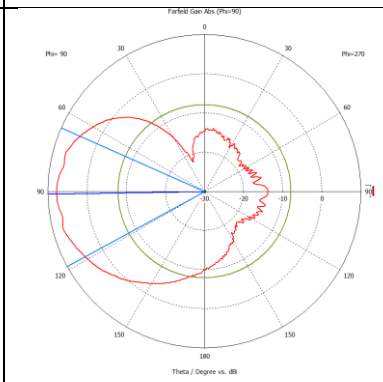	f_c = 5.78 GHz S_{11} = -22.196 Dir = 7.73 dBi. AW = 52.5 Deg SLL = -15.5 dB MLD = 91 Deg

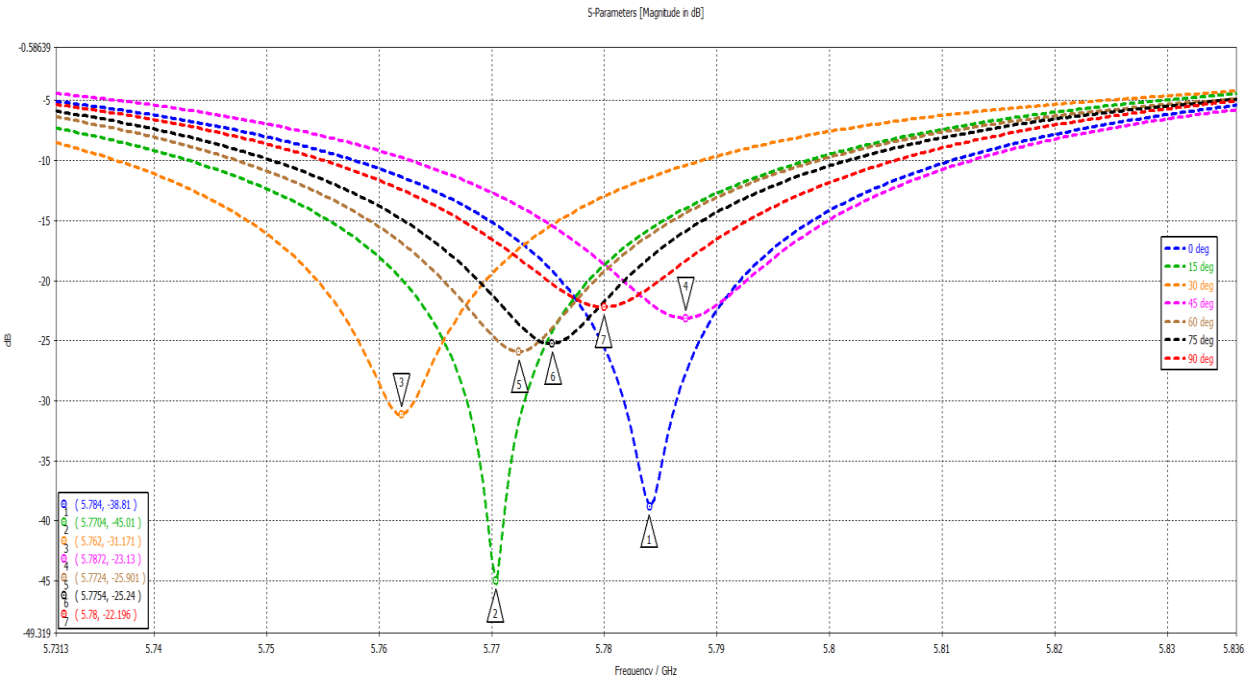

Figure 3.19 S_{11} of 2nd Approach: Double-plane patch with one director folding response.

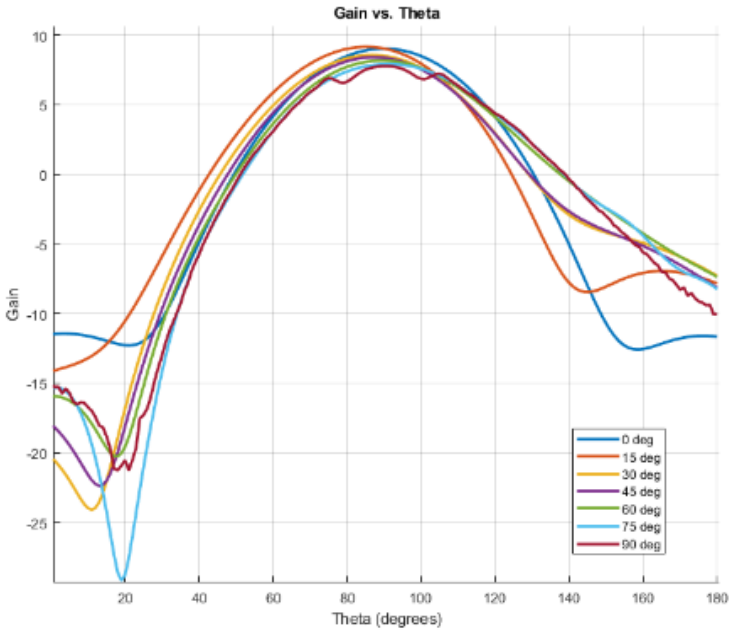

Figure 3.20 Gain vs theta 2nd Approach: Double-plane patch response.

3.4.2 Double-folded Director Study Response

In the current work, both directors are folded at different angles to investigate the response of a directional antenna. In the second instance, folding one side of the antenna at various angles, including 0°, 15°, 30°, 45°, 60°, and 90°, is the experimental process. The main goal of this inquiry is to thoroughly evaluate the effects of adjusting both directors on the operation and radiation pattern of the antenna. The study's findings will offer useful information on the best arrangements for both directors, permitting the creation of directional antennas with custom radiation patterns to satisfy application needs. To ensure the accuracy and applicability of the study's findings, as in the previous instance, strict adherence to antenna design standards and thorough consideration of the intended application are essential.

Table 3.8 2nd Approach: Double-plane, double-folded director simulation response.

Angle	Radiation Pattern	Polar Plot	Performance
15°	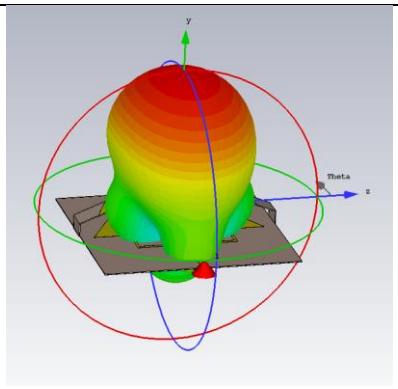	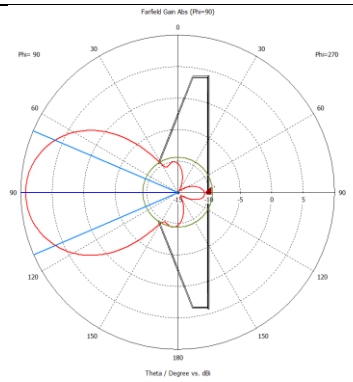	f_c = 5.7796 GHz. S_{11} = -44.077 Dir = 9.21 dBi. AW = 46.4 Deg. SLL =-18.6 dB MLD = 90 Deg
30°	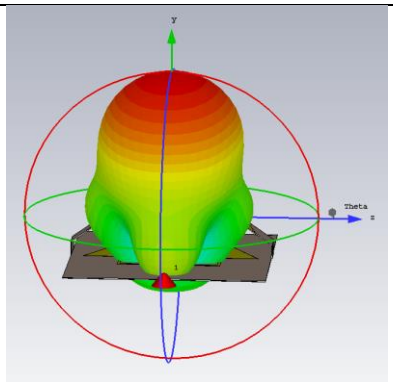	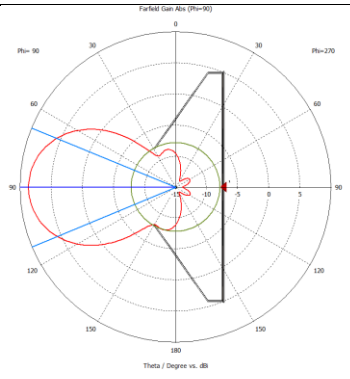	f_c = 5.7992 GHz S_{11} =-19.845 Dir = 8.54 dBi. AW = 45 Deg SLL = -16.5 dB MLD = 90 Deg

Table 3.8., Cont.

45°	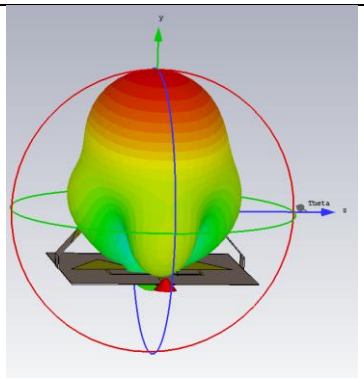	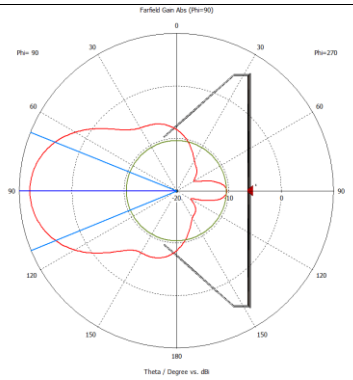	f_c = 5.798 GHz S_{11} = -15.338 Dir = 7.95 dBi. AW = 44 Deg SLL = -18.4dB MLD = 90 Deg
60°	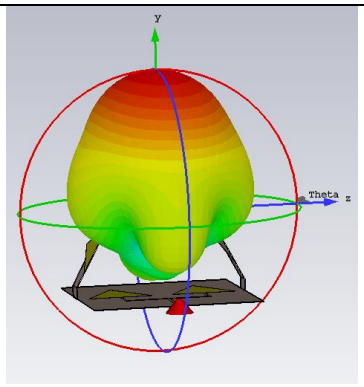	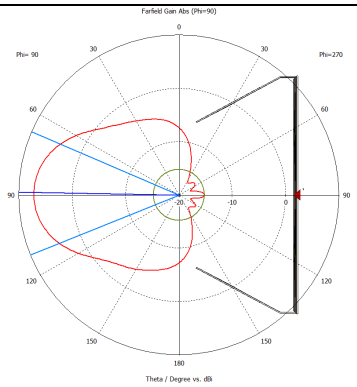	f_c = 5.7784 GHz S_{11} = -13.061 Dir = 7.15 dBi. AW = 45.3 Deg SLL = -22.3 dB MLD = 89 Deg
75°	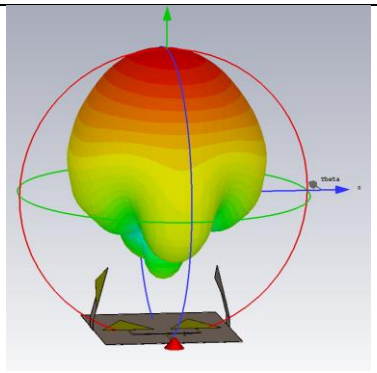	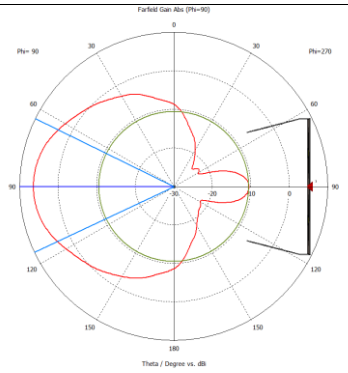	f_c = 5.7832 GHz S_{11} = -13.384 Dir = 6.44 dBi. AW = 51.4 Deg SLL = -16.9 dB MLD = 90 Deg
90°	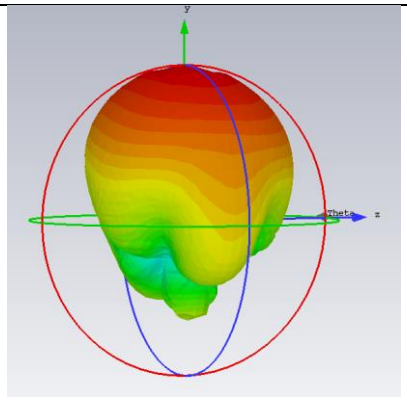	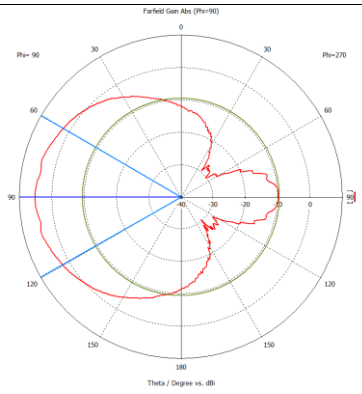	f_c = 5.7883 GHz S_{11} =-13.583 Dir = 5.24 dBi. AW = 59.9 Deg SLL = -14.6 dB MLD = 90 Deg

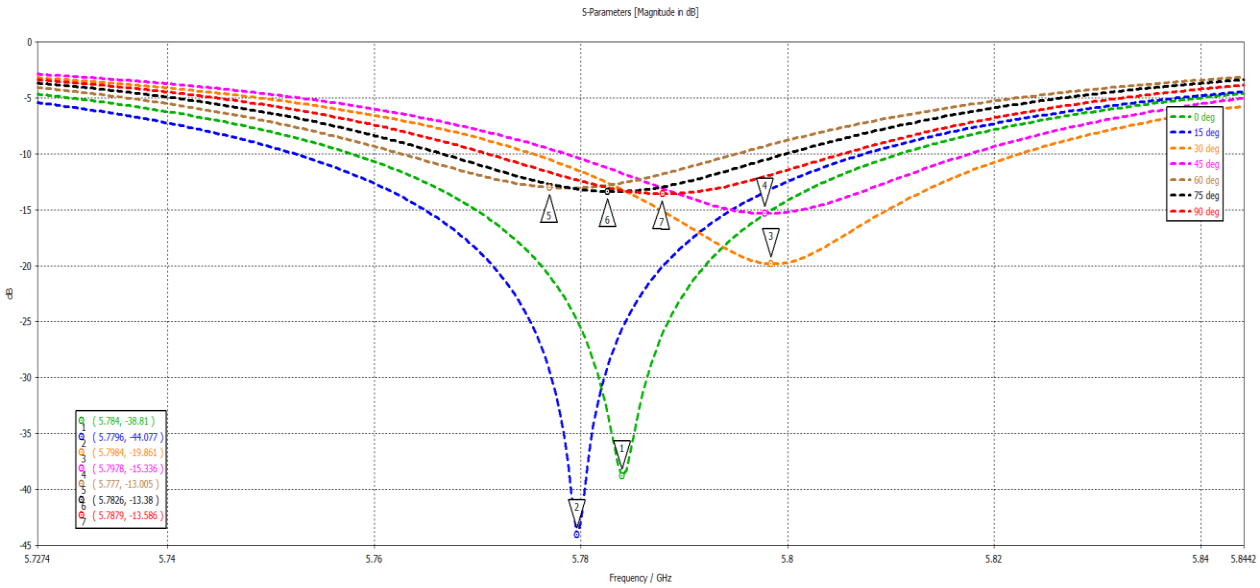

Figure 3.21 S_{11} of 2nd Approach: Double-plane patch, both folded directors response.

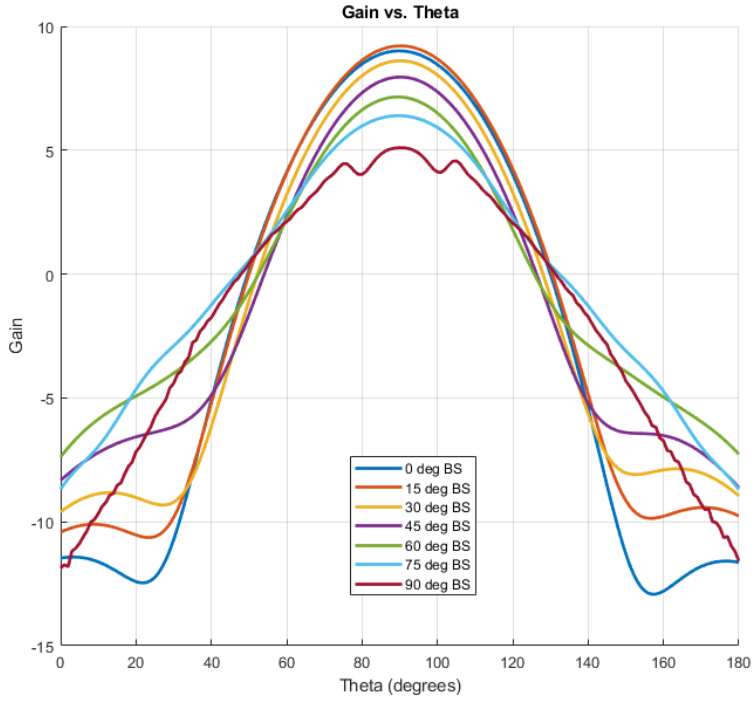

Figure 3.22 Gain vs theta, 2nd Approach both folded directors response.

CHAPTER IV

FABRICATION AND MEASUREMENTS

4.1 Fabrication Process with LPKF ProtoLaser Machine

The LPKF ProtoLaser U4 is a state-of-the-art laser-based rapid prototyping system that allows you to produce high-quality prototypes with an unmatched level of precision and accuracy. This machine combines the latest laser technology with sophisticated software and advanced automation features to deliver precise and efficient results. The LPKF ProtoLaser U4 boasts of advanced features like automatic focusing, high-resolution imaging, and real-time process monitoring, which make it an ideal tool for a wide range of applications, including PCB prototyping, SMT stencils, and microfluidics. With its compact design and user-friendly interface, it is an easy-to-use machine that can help you create complex structures with precision. The LPKF ProtoLaser U4 has several specifications that make it an excellent choice for prototyping. It uses a 355nm laser that can produce a spot size of 20 µm and has a maximum processing area of 229 x 305 mm. The laser system can handle a wide range of materials, including FR4, Rogers, ceramic, and polyimide, and can process substrates up to 3.2 mm thick. Additionally, the machine has a high-precision Z-axis system that can adjust the laser focus in real-time, allowing for precise cuts and etches. In conclusion, the LPKF ProtoLaser U4 is a powerful, versatile, and reliable laser-based prototyping system that is suitable for a wide range of applications. With its advanced

features and specifications, it can deliver precise and efficient results, making it an ideal choice for both small-scale and large-scale prototyping projects.

Figure 4.1 LPKF ProtoLaser U4.

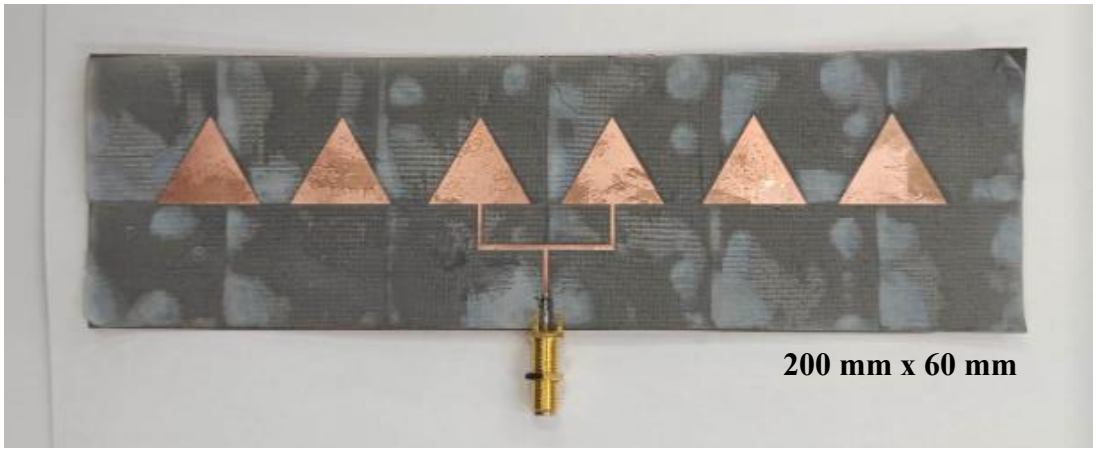

Figure 4.2 Fabricated 1st Approach: Single-plane folded patch.

Table 4.1 Software procedures for LPKF laser U4.

Procedure	Software Procedure
Start machine and wait until computer communicates with machine, once you check the lights in machine are ON can continue.	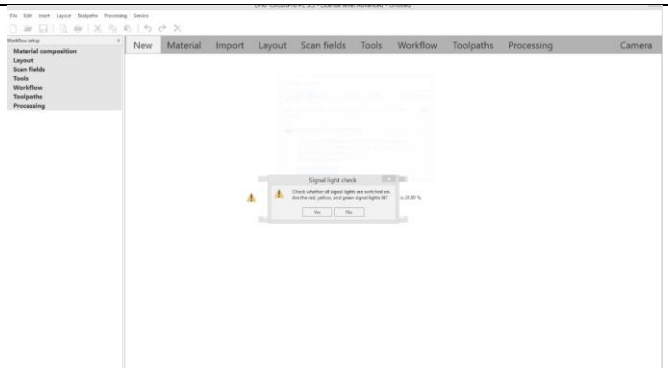
Select new project and the type of layer you are going to fabric.	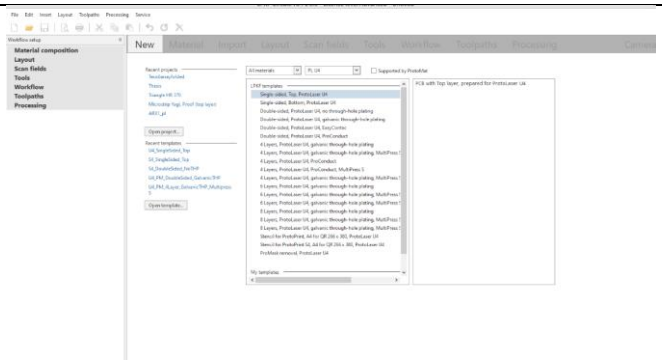
Give specifications of material to the software or select an existent one.	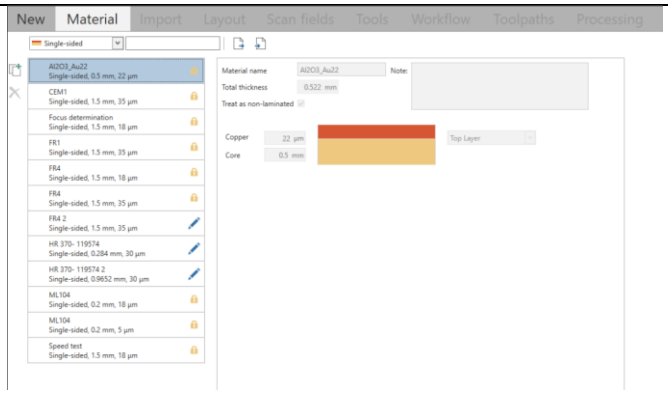
Import Gerber files and select appropriate target to them.	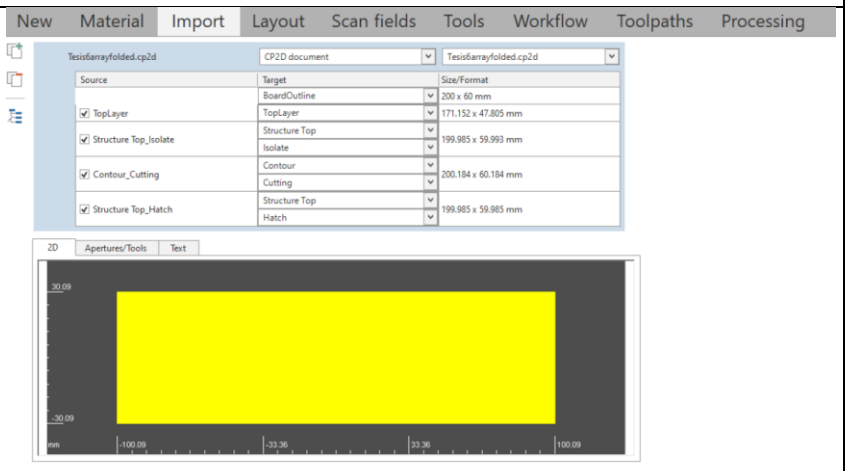

Table 4.1., Cont.

Select Layout and modify if necessary.	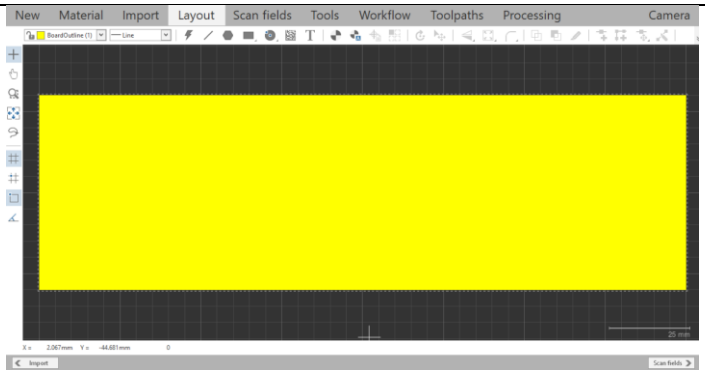
Select scan fields, here the software will compute automatically, but can be done by hand.	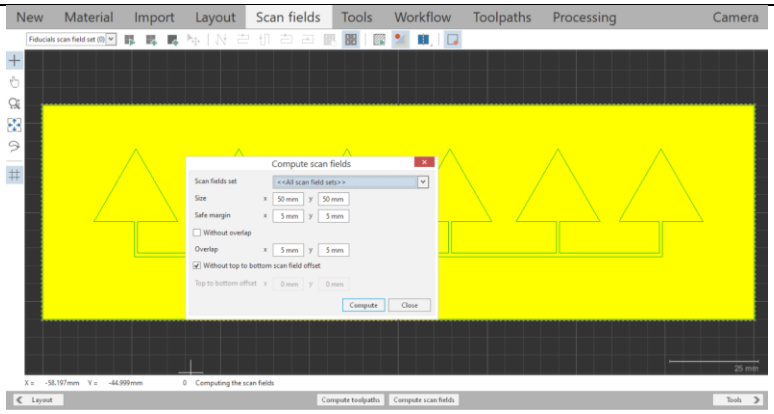
Once in tools, you can edit parameters of laser to create your own tools for cutting different materials.	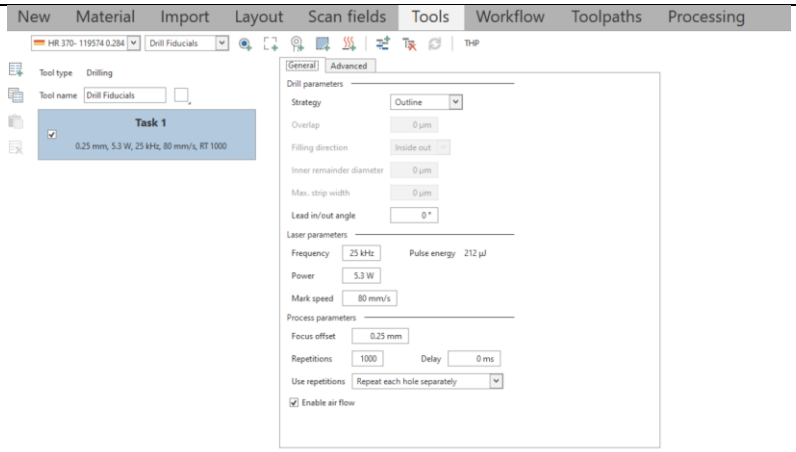
Verify that everything is in order. Also, if you want to miss a step, you can avoid it here in workflow.	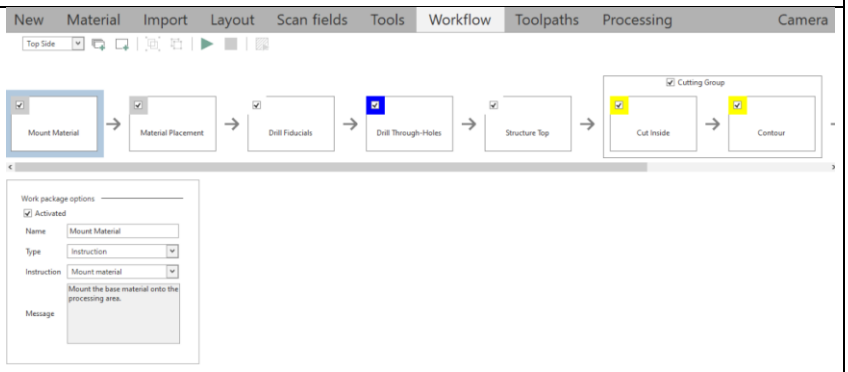

Table 4.1., Cont.

We select Toolpaths, software will compute automatically.	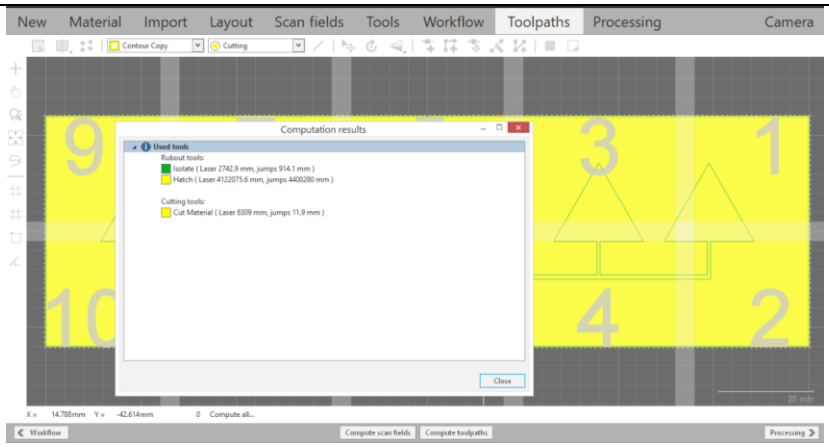
Now production can start. Here you can move your space work in the table.	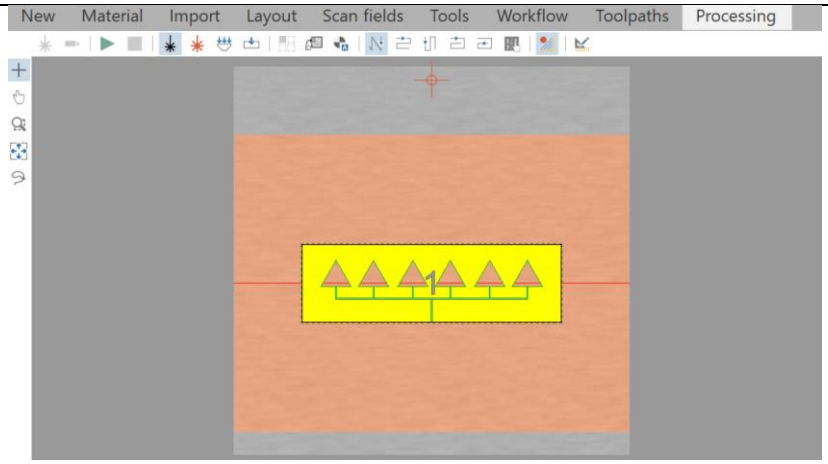

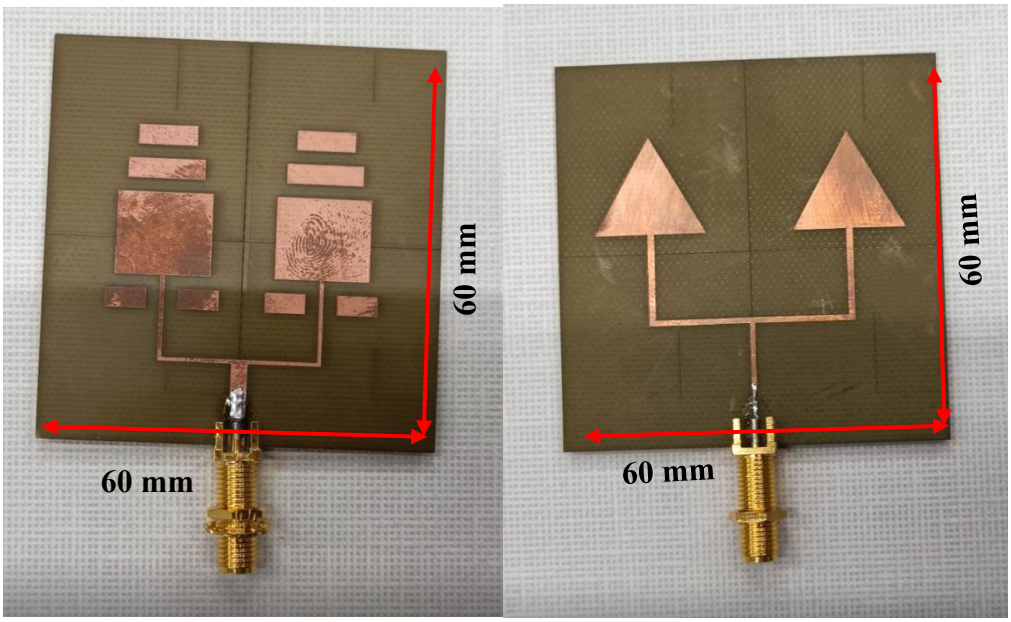

Figure 4.3 Antennas array fabricated with LPKF U4.

4.2 Measurements

A vector network analyzer (VNA) is a type of electronic test equipment used to measure the performance of high-frequency and microwave devices such as antennas, filters, amplifiers, and transmission lines. One of the key parameters that a VNA measures is the S_{11} parameter, which is a measure of how much power is reflected from a device or circuit back to the source when it is subjected to an incident signal.

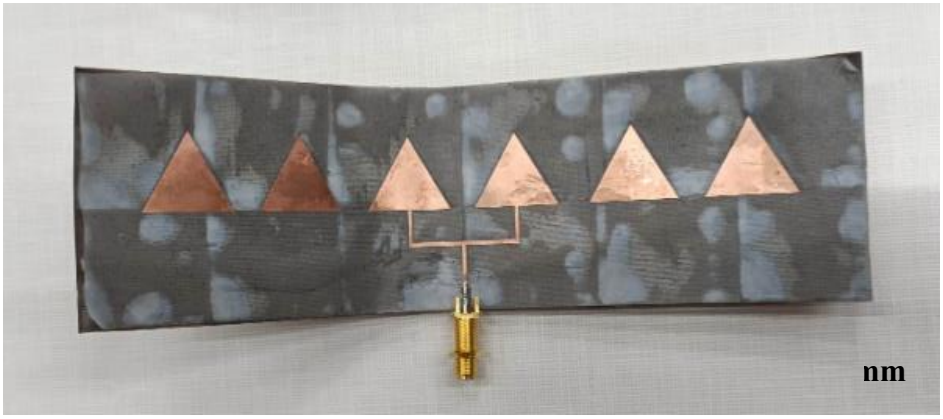

Figure 4.4 Fabricated 1st Approach: Single-plane folded patch when folds.

The VNA works by sending a known signal into the device or circuit being tested and measuring the signal that is reflected. By analyzing the reflected signal, the VNA can calculate various parameters, including the S_{11} parameter. The S_{11} parameter is represented as a complex number that has both magnitude and phase components, and it indicates how much of the incident signal is reflected and how much is transmitted through the device or circuit. The vector nature of the VNA comes from the fact that it is measuring both the magnitude and phase of the reflected signal, which allows for more accurate characterization of the device or circuit being tested. The VNA can also measure other parameters such as the S_{21} parameter, which measures the amount of

signal transmitted through the device or circuit, and the S_{12} and S_{22} parameters, which measure the amount of signal coupled between input and output ports of the device or circuit. The ability to measure these parameters makes the VNA a powerful tool for designing, testing, and optimizing high-frequency and microwave devices and circuits.

The Agilent 8720ES Network Analyzer is a high-performance RF and microwave network analyzer designed for accurate and reliable measurements of S-parameters. It operates in the frequency range of 50 MHz to 20 GHz and offers a wide range of measurement capabilities, including reflection coefficient (S_{11}), transmission coefficient (S_{21}), and phase measurements. It also has a fast sweep time and a high dynamic range, making it suitable for a wide range of applications in various industries, including aerospace, defense, telecommunications, and research and development. The Agilent 8720ES is known for its accuracy, reliability, and versatility, and has been widely used in both laboratory and field environments.

The Agilent 8720ES is a vector network analyzer (VNA) used for high-frequency measurements, while the HP 85052B 3.5 mm calibration kit is a set of precision components used to calibrate the VNA for accurate measurements. The calibration kit consists of a variety of coaxial standards with known properties, such as open circuit, short circuit, and load terminations, as well as a precision 3.5 mm calibration standard. These standards are used to calibrate the VNA's reference plane, remove systematic errors, and establish accurate measurement parameters. The Agilent 8720ES and HP 85052B work together by first connecting the calibration kit standards to the VNA's test ports. The VNA then measures the known properties of the calibration standards and uses this information to establish accurate measurement parameters for the test device connected to the VNA. By using the HP 85052B calibration kit, the Agilent 8720ES can provide

highly accurate and repeatable measurements for a variety of applications, including designing and testing microwave circuits and components.

Figure 4.5 Calibration kit HP 85052B.

Figure 4.6 Calibration kit components.

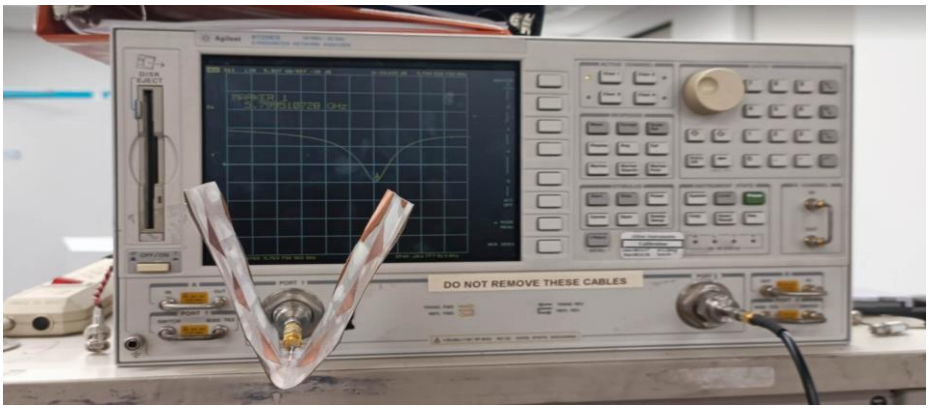

Figure 4.7 Testing setup.

Table 4.2 Calibration process of vector network analyzer.

Description	Calibration Process
Select "CAL" to open the calibration options.	
Select, "CALIBRATE MENU" to open options for different types of calibrations.	
Select "S11 1-PORT'' To start calibration in port 1	
Following screen shows a bottom for each tool.	

Table 4.2., Cont.

Connect each tool and select the bottom that correspond to each one.	
Once finished press "DONE:LOADS" and the calibration is ready.	

S_{11} Measurements with Spectrum Analyzer

Table 4.3 S11 parameters: comparison between simulation vs measured results.

 Single-Plane Patch Antenna Array	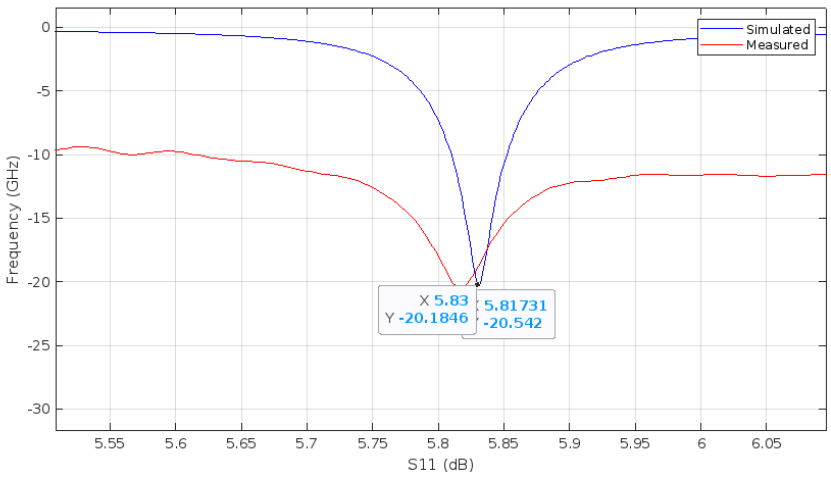

Table 4.3., Cont.

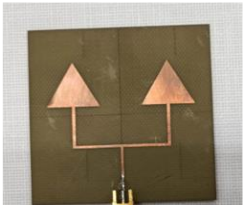 Triangle Microstrip Array	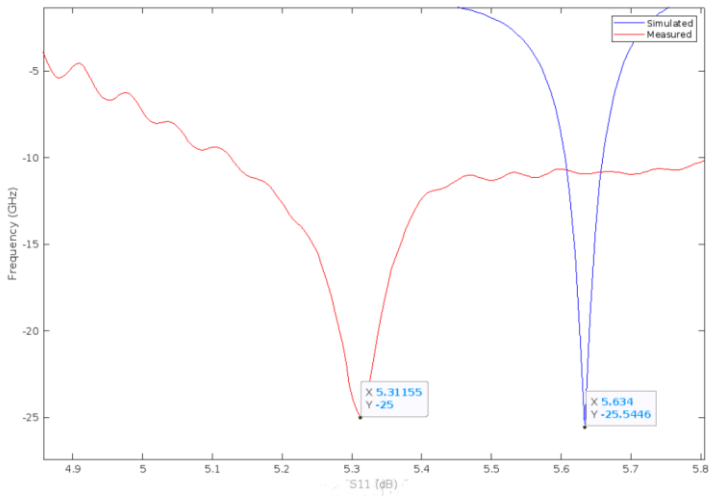
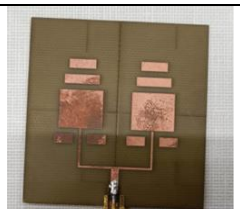 Microstrip Yagi-Uda Antenna Array	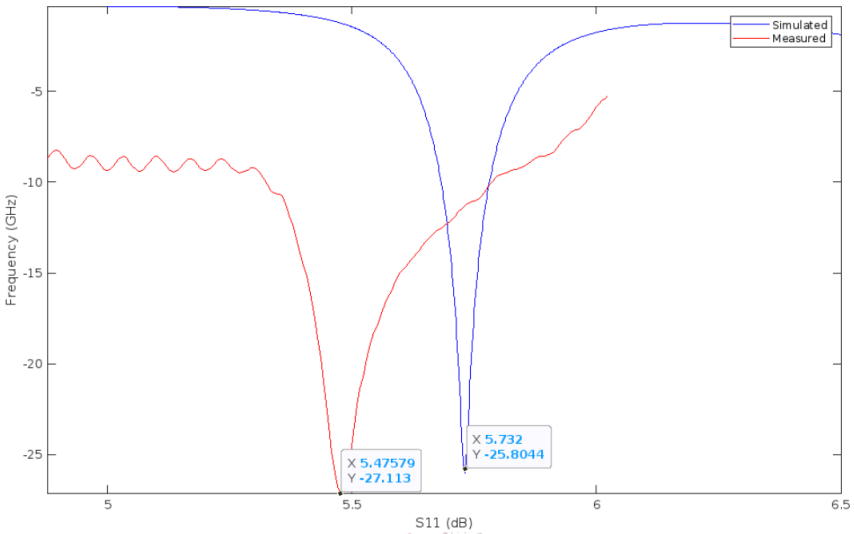

The table 4.1 represents the comparison between the simulated and measured results of the S_{11} parameters for three different types of antenna arrays: the single-plane patch antenna array, the triangle microstrip array, and the microstrip yagi-uda antenna array. The S_{11} parameter is a measure of the match between the antenna and the feed line. A lower S_{11} value in dB indicates a better match and thus less power reflected back to the source, implying a more efficient system.

For the single-plane patch antenna array, the simulated operational frequency was 5.81 GHz with an S_{11} value of -20.54 dB. The measured operational frequency was very close at 5.83 GHz, and the S_{11} value was slightly better at -20.18 dB.

The triangle microstrip array displayed a more noticeable difference between the simulated and measured results. The simulated operational frequency was 5.634 GHz with an S_{11} value of -25.54 dB, whereas the measured operational frequency was 5.31 GHz with a slightly worse S_{11} value of -25 dB.

In the case of the microstrip yagi-uda antenna array, the simulated operational frequency was 5.732 GHz with an S_{11} value of -25.8 dB. The measured operational frequency came in lower at 5.475 GHz, and the S_{11} value was worse at -27.11 dB.

These comparisons provide valuable insights into the accuracy and predictability of the simulations. They suggest that while simulations can give a good approximation of the antenna performance, actual measurements may vary due to factors not accounted for in the simulation, such as manufacturing tolerances, material inconsistencies, or environmental factors.

CHAPTER V

FINDINGS AND COMMENTS

This chapter analyzes the findings and conclusions derived from the investigation in detail. Rectangular and triangular array responses are compared in the first section of the chapter to draw important conclusions regarding their respective performances. The Single-Plane Folded Patch and the Double-Plane Patch are two different techniques that are covered in later parts. In the single-plane method, we examine the effects of folding the patch antenna with and without a microstrip line, investigating various configurations like one- or two-sided folding, and even simulating the influence of substrate curvature folding. With independent research concentrating on folding one director and both directors, the second strategy revolves around the folding of the Double-Plane Patch. Each segment in this chapter reveals crucial findings that elucidate our understanding of the topics under scrutiny, driving future research in this domain.

5.1 Rectangular and Triangular Array Response Comparison

This research introduces a groundbreaking approach in beam-steering antenna design, where the radiation pattern is tactically altered by modifying the geometry of the Microstrip Patch Array (MPA) and applying a folded substrate. This innovative method culminates in an antenna that achieves a Yagi-Uda radiation pattern by using a two-element triangular microstrip array,

deviating from the conventional rectangular patch array. This configuration results in significant improvements in gain and directivity by concentrating the radiation in a specific direction, outpacing the traditional rectangular patch design. The incorporation of parasitic elements in this unique structure, as detailed in earlier works [20], emulates the Yagi-Uda radiation pattern, therefore enhancing performance. Utilizing the CST software, this study provides a concrete demonstration that this new array configuration of triangular microstrips, combined with the use of parasitic elements and a folded substrate, offers superior performance. A highlight of the research is the design of an antenna optimized for Wi-Fi applications at 5.8 GHz and a simulation study scrutinizing the radiation pattern results under different substrate folding angles. This design, coupled with its simplicity, compactness, and cost-effectiveness, holds great potential for applications in telecommunications or satellite systems, and shows promise for exploration in conformal antenna applications.

In conclusion, this research showcases that increasing the number of parasitic elements in the substrate leads to an increase in impedance, potentially resulting in an impedance mismatch, yet it can simultaneously enhance the antenna's gain response. Simulation and measurement results clearly indicate that the triangular geometry can mimic, and even improve upon, the Yagi-Uda type response, even in the absence of parasitic elements. This makes the triangular geometry an optimal choice when a focused radiation pattern spike is required. The findings from this research offer significant implications for the design of future antenna systems, underscoring the potential benefits of exploring non-traditional geometries and configurations.

5.2 1st Approach: Single-Plane Folded Patch Antenna Study

The findings of this research demonstrate that the introduction of parasitic elements and the expansion of the substrate size led to improved S_{11} and gain responses. This suggests that these modifications significantly enhance the performance of the antenna, shedding light on effective strategies for the design and optimization of microstrip patch arrays. The enhancement in the antenna's ability to direct emitted energy and the improvement in efficiency show the potential advantages of this approach.

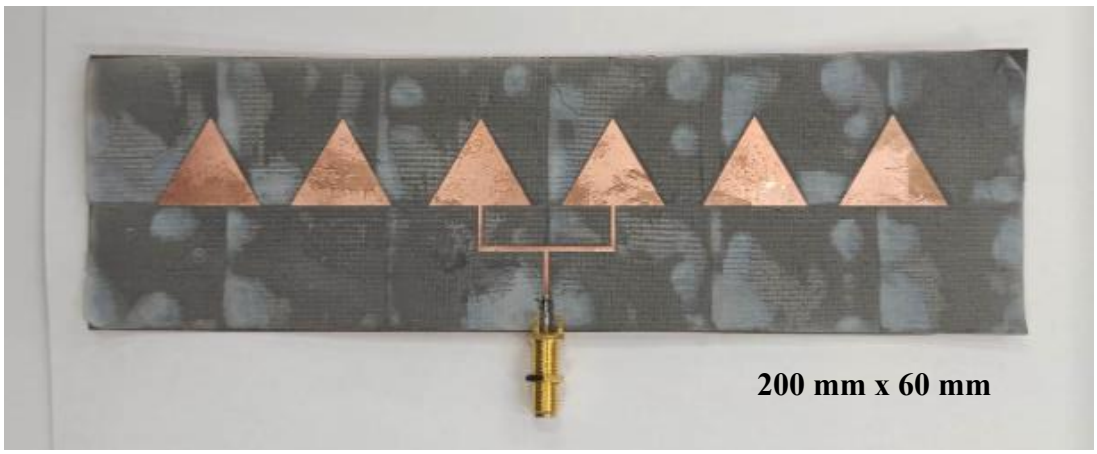

Figure 5.1 1st Approach: Single-plane folded patch.

5.2.1 One Side Unfolded Microstrip Line Findings and Comments

The results of this study delineate the impact of varying folding angles on the antenna's performance. As the substrate is folded at different angles - 15°, 30°, 45°, 60°, and 75° - without folding the microstrip line, the antenna exhibits specific operating frequencies, S_{11}reflection coefficients, gain, and beamwidth. For instance, at a folding angle of 15°, the antenna operates at 5.822 GHz with an S11 value of -19.43 dB, suggesting a good impedance match. Meanwhile, the gain is 8.019 dBi, and the beamwidth is 45.6°. As the folding angle is increased to 75°, the operating frequency shifts to 5.844 GHz, with the S_{11}value further decreasing to -20.046 dB, while the gain modestly increases to 8.7 dBi and the beamwidth contracts to 36.6°.

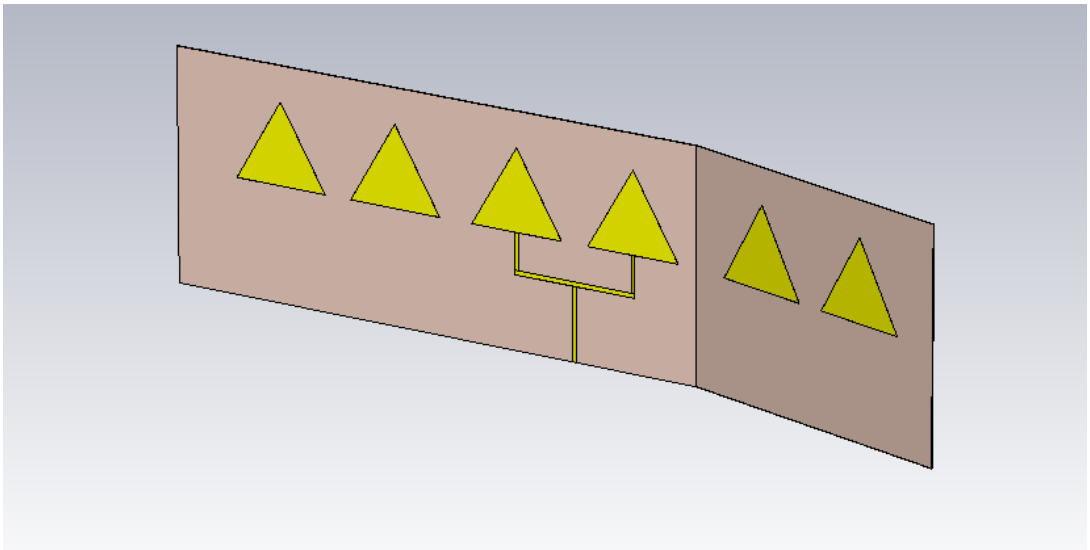

Figure 5.2 1st Approach: Single-plane folded patch one side.

Findings from this research provide clear evidence that folding the substrate at varying angles can effectively shape the antenna's radiation pattern, leading to increased gain. Additionally, the S_{11} reflection coefficient does not exhibit substantial fluctuations across the different folding angles, suggesting the stability of impedance matching. This consistency in the S_{11} value and the improved gain signify the potential efficacy of this novel approach to antenna design.

In conclusion, this research significantly contributes to the field of antenna design by showcasing the benefits of manipulating substrate folding angles. The systematic examination of the performance metrics at various folding angles underscores the feasibility and effectiveness of this approach, potentially guiding future design enhancements.

5.2.2 Two Sides Unfolded Microstrip Line Simulation Response

The results depict a unique interplay between the folding angles including 15°, 30°, 45°, 60°, and 75° and the corresponding operating frequencies, S_{11} reflection coefficients, and directivity. For instance, at a 15° folding angle, the antenna operates at 5.828 GHz with an

S11

value of -18.968 dB, indicating a satisfactory impedance match, and a directivity of 10.28 dBi. As the folding angle increases to 75°, the operating frequency slightly changes to 5.8364 GHz, with a slightly improved S_{11} value of -19.157 dB and a directivity of 10.48 dBi.

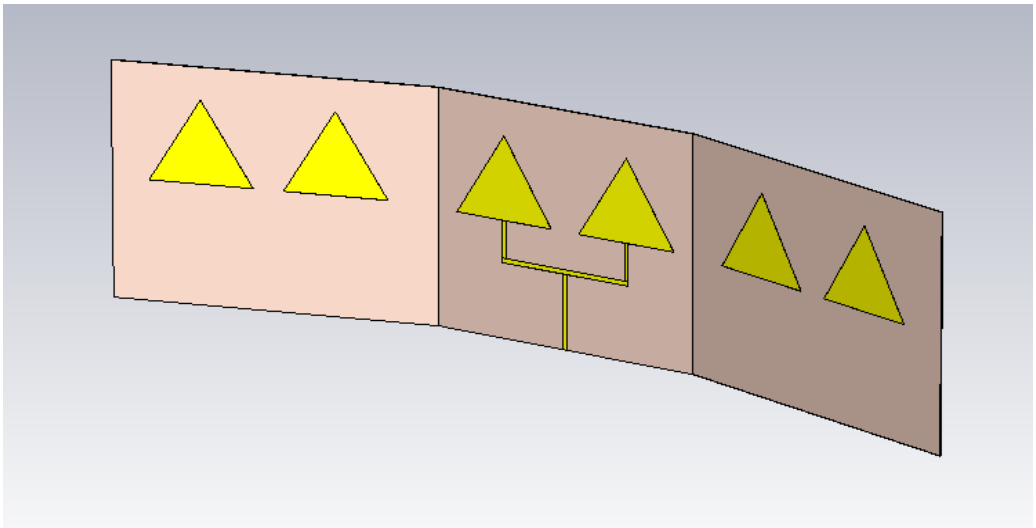

Figure 5.3 1st Approach: Single-plane folded patch, two side folded.

The findings reveal that the S_{11}value remains relatively stable across different folding angles, indicating minimal shifts in frequency and no substantial changes in reflection. Furthermore, it's observed that the substrate reflection of the radiation pattern increases when both sides are folded, leading to a corresponding increase in gain. This suggests that manipulating the folding angle of the substrate on both sides can effectively control the antenna's radiation pattern and enhance its performance.

In conclusion, the study presents significant insights into optimizing antenna performance through strategic manipulation of substrate folding angles. The empirical evidence demonstrates that even without folding the microstrip line, the use of passive elements and control over substrate folding can yield improved antenna gain and stable impedance match.

5.2.3 One Side Folded Microstrip Line Simulation Response

The simulation findings provide insightful information regarding the performance of an antenna when the microstrip line is folded into one side of the substrate. Detailed investigations are carried out at various folding angles - 15°, 30°, 45°, 60°, and 75°. Specific operating frequencies, S_{11}reflection coefficients, and directivity (in dBi are associated with each of these angles. For instance, at a 15° folding angle, the antenna operates at 5.8402 GHz, has an S_{11} value of -18.709 dB, and exhibits a directivity of 10.08 dBi. As the folding angle is further increased to 75°, the operating frequency becomes 5.8404 GHz, with an S_{11} value of -22.472 dB and a directivity of 10.79 dBi.

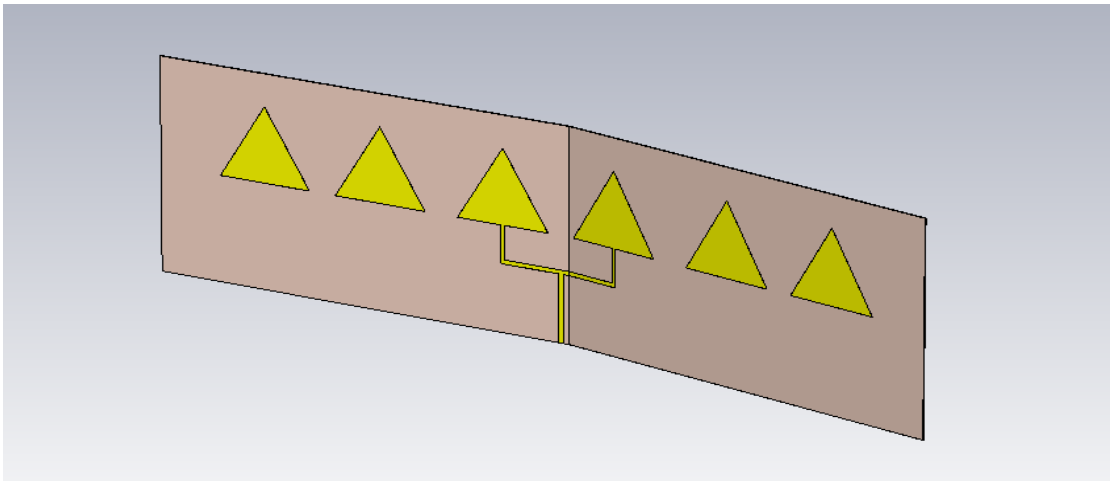

Figure 5.4 1st Approach: Single-plane folded patch, one side folding with microstrip line.

These findings reveal a few critical aspects. One, folding the microstrip line has minimal effects on the frequency response, with the frequency remaining relatively stable across different folding angles. However, this action does have an impact on the S_{11} parameters' reflection. This indicates that folding the microstrip line can alter the antenna's impedance matching.

In conclusion, this study provides valuable insights into the effects of folding the microstrip line into the substrate on the performance of the antenna. The results can be instrumental in the design and optimization of antenna systems, particularly those that require control over impedance matching.

5.2.4 Two Sides Folded Microstrip Line Simulation Response

With the inclusion of active microstrip line folding, the simulation results offer a thorough examination of the antenna performance when the substrate is folded on both sides. The analysis captures the behavior of the antenna at various folding angles. S_{11} reflection coefficients, operational frequencies, and directivity measurements (in dBi are given for each angle. For example, at a 15° folding angle, the antenna operates at 5.824 GHz, with an S_{11} value of -21.892 dB and a directivity of 9.748 dBi. As the folding angle increases to 75°, the operating frequency slightly shifts to 5.8258 GHz, while the S_{11} value improves significantly to -6.9285 dB, and the directivity measures at 9.696 dBi.

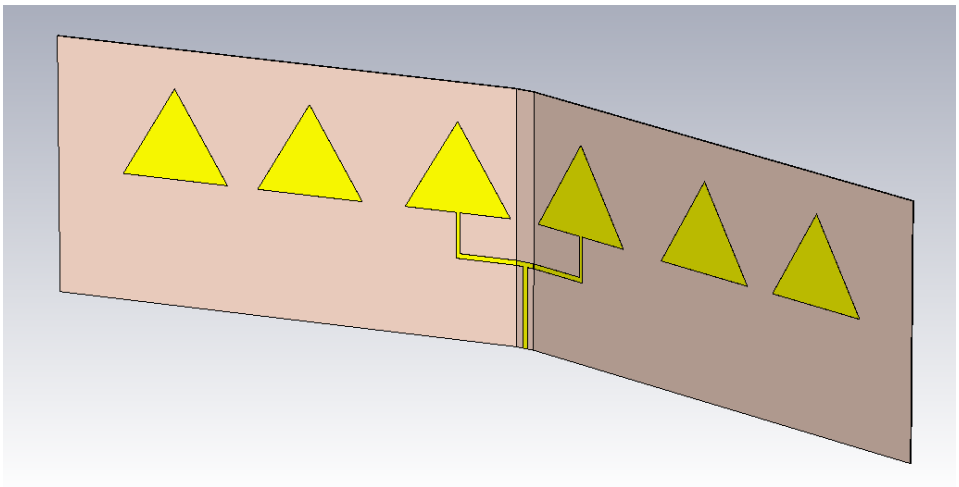

Figure 5.5 1st Approach: Single-plane, two side folding with microstrip line.

The findings reveal a minor frequency shift across different folding angles, indicating the stability of the frequency response even with changes in the substrate folding. However, there is a considerable change in the S_{11} parameters. This suggests that while folding the microstrip line on both sides of the substrate may have a limited impact on the operating frequency, it profoundly influences the impedance match. The impact varies with the degree of folding, signifying a direct relationship between the folding angle and the S_{11} value.

5.2.5 Curvature Folded Substrate

In conclusion, the simulation data reaffirms the inherent benefits of using a circular folding substrate in antenna design. This form enhances beam directionality and radiation patterns, qualities that are indispensable in scenarios where high-gain and well-defined radiation patterns are essential. The presented work serves as a testament to the potential of exploring diverse geometries in antenna design.

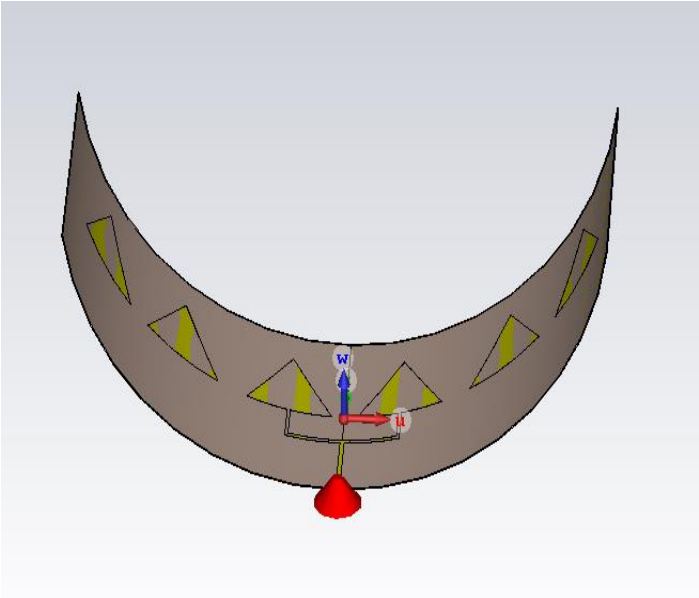

Figure 5.6 Semicircular folding 1st Approach: Single-plane folded patch.

The data provides a crucial point of departure in the quest to optimize circular folding substrate designs for a plethora of wireless communication systems and related applications. Notably, operating at 5.819 GHz, the antenna exhibits an admirable S_{11} value of -18.57 dB, illustrating a commendable impedance match. Further, the directivity of 11.86 dBi underscores the antenna's proficient ability to concentrate and guide radiated energy.

Overall, these insights form a cornerstone in developing efficient and effective antenna solutions, thereby enhancing the overall performance and reliability of communication systems. While this research serves as proof of concept, the extensive simulation results provide a promising outlook for practical applications.

5.3. 2nd Approach: Double-Plane Patch

The double-plane patch approach, as explored in Section 3.4, pivots on a four-element antenna array design with directors parallel to the driven elements' plane. The configuration of this array plays a vital role in molding the radiation pattern and overall performance of the antenna, thereby holding significant value in antenna engineering.

Comprising the array are the driven element, which is the primary radiating element, and the directors which are passive elements. The inclusion of these directors adjacent to the driven element proves instrumental in enhancing radiation in the preferred direction, and in augmenting the gain and directivity of the antenna.

The extensive simulation study conducted on this four-element antenna array provides crucial insights into the array's performance under various operational circumstances. This research holds the potential to aid the optimization of design parameters and thus boost the

antenna's response and radiation attributes. Ultimately, the knowledge gleaned from this study paves the way for the development of high-performing antenna arrays, fit for a broad range of communication applications, spanning satellite communication, radar systems, to wireless communication systems and more.

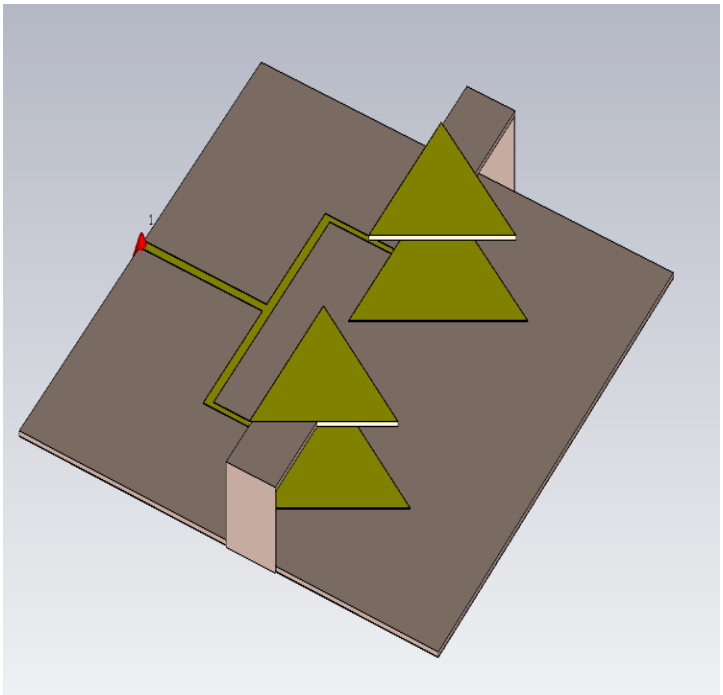

Figure 5.7 2nd Approach: Double-plane patch, directors parallel to the plane of driven elements.

5.3.1 Single-Folded Director Study Response

The conclusion derived from the simulations of antenna response by adjusting one director element at various angles, ranging from 15 to 90 degrees, offers valuable insights into the design and operation of antenna arrays. The impact of these adjustments on the antenna's operational characteristics, such as frequency, S_{11} reflection coefficient, and directivity, is significant and should be considered in antenna design. The data demonstrated distinct shifts in operational frequency with changes in the angle of the director. For instance, at a 15-degree folding angle, the

operating frequency was 5.7704 GHz, which shifted to 5.762 GHz at 30 degrees, then to 5.7872 GHz at 45 degrees, and so on. Notably, the shifts in frequency were substantial, thereby impacting the antenna's suitability for specific communication systems.

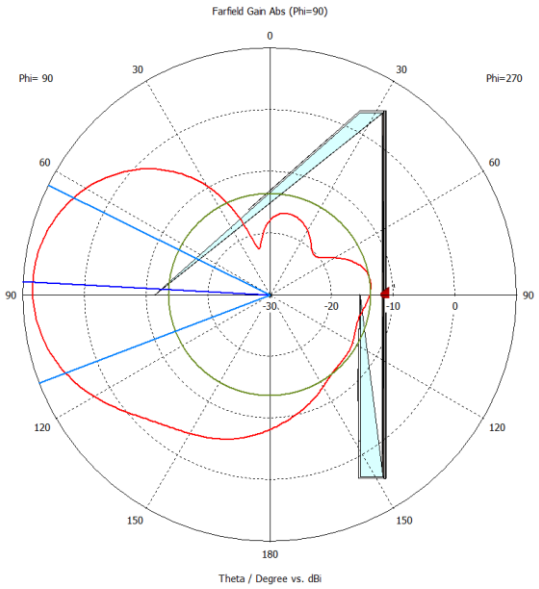

Figure 5.8 2nd Approach: Double-plane patch, single side folding.

Further, S_{11} reflection coefficients, indicative of the antenna's impedance match, changed significantly with every adjustment in the director's angle. At 15 degrees, the S_{11} value was -45.237 dB, which increased to -31.171 dB at 30 degrees, and continued to fluctuate with further angular adjustments. The shifts in S_{11} indicate changes in the antenna's efficiency in power transfer. The antenna's directivity, a measure of its ability to concentrate energy in a specific direction, also exhibited variations with different angles of the director. This parameter ranged from a high of 9.14 dBi at 15 degrees to a low of 7.73 dBi at 90 degrees, indicating changes in the concentration of radiated energy as the angle changed. To sum up, the study provides evidence that alterations in the director's angle can significantly influence the operational characteristics of an antenna array.

By gaining insights into these effects, antenna designers can better optimize performance, enhancing the overall functionality and efficiency of communication systems.

5.3.2 Double-folded Director Study Response

The simulation study that folded both directors at various angles in a directional antenna brought forward some interesting observations. In particular, the behavior of operational frequency, S_{11}, reflection coefficient, and gain (directivity showed significant shifts at different folding angles, ranging from 15° to 90°. Starting with the operational frequency, the study found significant variations with the change in the folding angle of the directors. The frequency ranged from 5.7796 GHz at 15° to 5.798 GHz at 45°, finally reaching 5.7883 GHz at 90°. These variations in frequency could impact the antenna's performance, affecting its suitability for specific communication systems.

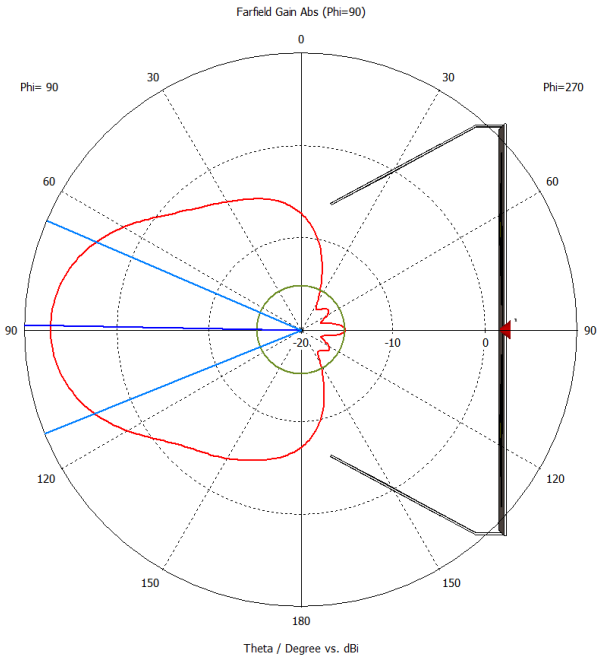

Figure 5.9 2nd Approach: Double-plane patch, double side folding.

Secondly, the S11 reflection coefficient, which indicates how well the antenna is matched to its feed line and thus reflects power back to the source, also changed considerably with the director's folding angle. From an S11 value of -44.077 dB at 15°, it increased to -13.583 dB at 90°. These changes suggest fluctuations in the antenna's efficiency in power transfer. The gain or directivity of the antenna, showing its ability to focus energy on a specific direction, showed considerable changes with the angle of the directors. The gain measurements ranged from 9.21 dBi at 15° to a significantly lower 5.24 dBi at 90°. This suggests that the concentration of radiated energy changes as the angle of the directors is adjusted.

In conclusion, this study suggests that changing the angles of both directors can considerably impact the antenna's performance metrics. Such insights can provide valuable input for antenna design, allowing customization of radiation patterns and optimization of antenna performance for different applications.

REFERENCES

[1] Balanis, C. A., 2016. Antenna Theory: Analysis and Design. Arizona: John Wiley & Sons, Inc.. Elliott, R. S., 2003. ANTENNA THEORY. Revised Edition ed. Los Angeles, California: JOHN WILEY & SONS, INC.

[2] Beneck, R. J. et al. Reconfigurable antennas: a review of recent progress and future prospects for next generation. Prog. Electromag. Res. 171, 89–121 (2021).

[3] Bernhard and C. Balanis, Reconfigurable Antennas (Synthesis Lectures on Antennas and Propagation), 1st ed. San Rafael, CA, USA: Morgan & Claypool, 2006.

[4] Bernhard, J. T. Reconfigurable antennas. Synth. Lect. Antennas 2, 166 (2007).

[5] Biswas, A., Zekios, C. L. & Georgakopoulos, S. V. Transforming single-band static FSS to dual-band dynamic FSS using origami. Sci. Rep. 10, 13884 (2020).

[6] Bossard, J. A. et al. Mitigating field enhancement in metasurfaces and metamaterials for high-power microwave applications. IEEE Trans. Antennas Propag. 64, 5309–5319 (2016).

[7] Braaten et al., "A Self-Adapting Flexible (SELFLEX) Antenna Array for Changing Conformal Surface Applications," in IEEE Transactions on Antennas and Propagation, vol. 61, no. 2, pp. 655-665, Feb. 2013, doi: 10.1109/TAP.2012.2226227.

[8] Bruce, E. & Beck, A. C. Experiments with directivity steering for fading reduction. Proc. Inst. Radio Eng. 23, 357–371 (1935).

[9] Byford, K. Park, P. Chahal, and E. Rothwell, “Frequency reconfigurable patch antenna array,” Electron. Lett., vol. 51, no. 21, pp. 1628–1630, Oct. 2015.

[10] Christodoulou, C. G., Tawk, Y., Lane, S. A. & Erwin, S. R. Reconfigurable antennas for wireless and space applications. Proc. IEEE 100, 2250–2261 (2012).

[11] Espinal, F.A., Huff, G.H., Pallampati, S., Sessions, D., Fuchi, K., Bazzan, G., Seiler, S.R., Buskohl, P.R., Cook, A.B. and Gillman, A.S. (2020), Circularly-polarised origami-inspired folding patch antenna sub-array. IET Microw. Antennas Propag., 14: 1262-1271.

[12] Georgakopoulos et al., "Origami Antennas," in IEEE Open Journal of Antennas and Propagation, vol. 2, pp. 1020-1043, 2021, doi: 10.1109/OJAP.2021.3121102.

[13] Gregory, M. D. et al. A low cost and highly efficient metamaterial reflector antenna. IEEE Trans. Antennas Propag. 66, 1545–1548 (2018).

[14] Hamza, C. L. Zekios and S. V. Georgakopoulos, "A Thick Origami Reconfigurable and Packable Patch Array With Enhanced Beam Steering," in IEEE Transactions on Antennas and Propagation, vol. 68, no. 5, pp. 3653-3663, May 2020.

[15] Haupt, R. L. & Lanagan, M. Reconfigurable antennas. IEEE Antennas Propag. Mag. 55, 49–61 (2013).

[16] Hwang, G. Kim, S. Kim and N. S. Jeong, "Origami-Inspired Radiation Pattern and Shape Reconfigurable Dipole Array Antenna at C-Band for CubeSat Applications," in IEEE Transactions on Antennas and Propagation, vol. 69, no. 5, pp. 2697-2705, May 2021.

[17] Ismail, Nuraiza & Ali, M.T. & Dzulkefli, N.N.S.N. & Abdullah, Rusli & Omar, Sarkawt. (2012). Design and analysis of microstrip Yagi antenna for Wi-Fi application. 283-286. 10.1109/APACE.2012.6457677.

[18] Lang, R. J., Tolman, K. A., Crampton, E. B., Magleby, S. P. & Howell, L. L. A review of thickness-accommodation techniques in origamiinspired engineering. Asme. Appl. Mech. Rev. 70, 010805 (2018).

[19] Li, Y. Shi, H. Shen, and L. Li, “A characteristic-mode-based polarization–reconfigurable antenna and its array,” IEEE Access, vol. 6, pp. 64587–64595, 2018.

[20] Lyke, J. C., Christodoulou, C. G., Vera, G. A. & Edwards, A. H. An introduction to reconfigurable systems. Proc. IEEE 103, 291–317 (2015).

[21] Mailloux, Phased Array Antenna Handbook. Norwood, MA, USA: Artech House, 2005.

[22] Miranda, F. A commentary on reconfigurable communications systems in support of NASA mission. Workshop on Origami Antennas and Electromagnetics and Kickoff Meeting for Center for Physically Reconfigurable and Deployable Multifunctional Antennas (2018).

[23] Mohamadzade et al., "A Conformal, Dynamic Pattern-Reconfigurable Antenna Using Conductive Textile-Polymer Composite," in IEEE Transactions on Antennas and Propagation, vol. 69, no. 10, pp. 6175-6184, Oct. 2021, doi: 10.1109/TAP.2021.3069422.

[24] Parkinson, M. B., Jensen, B. D. & Kurabayashi, K. Design of compliant force and displacement amplification micro-mechanisms. in Proceedings of the ASME 2001 International Design Engineering Technical Conferences and Computers and Information

in Engineering Conference. Vol. 2B: 27th Design Automation Conference, 741–748 (2001).

[25] Rubio et al., "An Origami-Inspired Foldable Reflectarray on a Straight-Major Square-Twist Pattern," 2021 IEEE 21st Annual Wireless and Microwave Technology Conference (WAMICON), Sand Key, FL, USA, 2021, pp. 1-4, doi: 10.1109/WAMICON47156.2021.9443629.

[26] Rubio, A. J. et al. A foldable reflectarray on a hexagonal twist origami structure. IEEE Open J. Antennas Propag. 2, 1108–1119 (2021).

[27] Seiler et al., "Physical reconfiguration of an origami-inspired deployable microstrip patch antenna array," 2017 IEEE International Symposium on Antennas and Propagation & USNC/URSI National Radio Science Meeting, San Diego, CA, USA, 2017.

[28] Shah, M. M. Tentzeris and S. Lim, "Low-Cost Circularly Polarized Origami Antenna," in IEEE Antennas and Wireless Propagation Letters, vol. 16, pp. 2026-2029, 2017, doi: 10.1109/LAWP.2017.2694138.

[29] Syed Imran Hussain Shah, Sungjoon Lim, Review on recent origami inspired antennas from microwave to terahertz regime, Materials & Design, Volume 198, 2021, 109345, ISSN 0264-1275, https://doi.org/10.1016/j.matdes.2020.109345.

[30] X. Liu, C. L. Zekios, and S. V. Georgakopoulos, “Analysis of a packable and tunable origami multi-radii helical antenna,” IEEE Access, vol. 7, pp. 13003–13014, 2019.

[31] Xu et al., "Wide Solid Angle Beam-Switching Conical Conformal Array Antenna With High Gain for 5G Applications," in IEEE Antennas and Wireless Propagation Letters, vol. 17, no. 12, pp. 2304-2308, Dec. 2018, doi: 10.1109/LAWP.2018.2873703.

[32] Yao and S. V. Georgakopoulos, “Origami segmented helical antenna with switchable sense of polarization,” IEEE Access, vol. 6, pp. 4528–4536, 2018.

[33] Yao, S.&Georgakopoulos, S. V.Origami segmented helical antenna with switchable sense of polarization. IEEE Access 6, 4528–4536 (2018). Shah,S. I.H., Tentzeris,M.M. & Lim,S. Low-costcircularlypolarized.

[34] Yao, X. Liu, and S. V. Georgakopoulos, “Morphing origami conical spiral antenna based on the nojima wrap,” IEEE Trans. Antennas Propag., vol. 65, no. 5, pp. 2222–2232, May 2017.

[35] Yellowhorse, A. & Howell, L. L. Three approaches for managing stiffness in origami-inspired mechanisms. in Proceedings of the ASME 2018 International Design Engineering Technical Conferences and Computers and Information in Engineering Conference. Vol. 5B (2018).

[36] Zhang, G. Huff, J. Feng, and J. Bernhard, “A pattern reconfigurable microstrip parasitic array,” IEEE Trans. Antennas Propag., vol. 52, no. 10, pp. 2773–2776, Oct. 2004.

[37] Zhu, H. L., Liu, X. H., Cheung, S.W. & Yuk, T. I. Frequencyreconfigurable antenna using metasurface. IEEE Trans. Antennas Propag. 62, 80–85 (2014).

BIOGRAPHICAL SKETCH

Luis Alonso Hernandez Galvan, a pioneering mechatronics engineer, was born and raised in Nuevo Laredo, Tamaulipas, Mexico. His academic journey began at a practical high school, where he showed an early aptitude for complex problem-solving, ultimately earning a degree as a mechatronics technician. From there, his unwavering commitment to the field led him to the Tecnologico Nacional de Mexico, Campus Nuevo Laredo, where he pursued and obtained a bachelor's degree in mechatronics from 2014 to 2019.

After graduation, he quickly transitioned into the professional world as a research assistant at the University of Texas Rio Grande Valley (UTRGV). There, he worked on the Blue Energy project under the guidance of Dr. Yang in 2019. This experience allowed him to contribute his skills to practical applications and gain invaluable experience in the field of renewable energy.

By 2022, Hernandez expanded his professional contributions by joining the Center of Advanced Radio Astronomy at UTRGV as a research assistant under the tutelage of Dr. Creighton. In August 2023, he earned his Master of Science in Engineering, specializing in Electrical Engineering, at UTRGV. Luis Alonso Hernandez Galvan continues to leverage his academic acumen and practical experience to innovate and advance in the ever-evolving field of engineering. You can make contact at hluis1368@gmail.com.